Asymptotically exact formulation of superfluid turbulence with discrete topological defects at all continuum scales

Demosthenes Kivotides
Strathclyde University, Glasgow, Scotland G1 1XQ, United Kingdom

(Received 2 February 2026; accepted 13 April 2026; published 7 May 2026)

We present an asymptotically exact continuum formulation of finite-temperature superfluid turbulence that consistently couples quantized vortex filaments to the turbulent normal fluid across all continuum scales. The key ingredient is the explicit linear-response theory (LRT) Stokes microhydrodynamic response generated by the line-supported mutual-friction and Iordanskii forces acting on the normal fluid. This response yields hydrodynamic-interaction (HI)-resolved vortex dynamics in which the filament-sampled normal-fluid velocity includes the full disturbance flow. Analytical solutions for canonical configurations (parallel and antiparallel line pairs and a vortex ring) show that microhydrodynamic coupling renormalizes defect motion and can permit stalling and reversal phenomena excluded in freely draining defect dynamics. To bridge the prohibitive separation between microhydrodynamic and turbulent scales in practical calculations, we couple a filtered Navier-Stokes description of the normal component to a concurrent low-Reynolds-number (LRT/Stokes) microflow solver. In the filtered normal-fluid equations the LRT microflow enters in two distinct, explicit ways: (i) it generates a deterministic residual (subfilter) stress from the subcutoff microflows, and (ii) it supplies hydrodynamically consistent mutual-friction and Iordanskii forcing via the HI-resolved defect reaction forces. The resulting hydrodynamic-scale system resolves inertial turbulence down to the physical cutoff set by viscous damping and two-fluid coupling. The formulation is boundary-condition agnostic—periodic, unbounded, and wall-bounded geometries enter only through the Stokes mobility returned by the solver—and is asymptotically exact in the scale-separated limit as a consequence of the overdamped Stokes/LRT response, which relaxes rapidly compared with the smallest resolved turbulent timescales. We indicate a detailed algorithmic procedure implementing the new formulation.

DOI: 10.1103/xp9w-f6ks

I. INTRODUCTION

Spontaneous symmetry breaking [1], the associated order parameter, and the Goldstone modes arising from its phase fluctuations are key dynamical phenomena in statistical and quantum physics. In the nonrelativistic, Galilean-invariant quantum case, a strongly interacting, spin-zero liquid (as realized in helium-4) can spontaneously break its global $U(1)$ symmetry, so that the Heisenberg field operator acquires a nonzero expectation value in the ground state, defining a condensate [2–4]. Denoting the exact many-body ground state in the broken-symmetry phase by $|\Omega\rangle$, the condensate order parameter is

$$\Phi(\mathbf{x}) \;=\; \langle\Omega|\hat{\psi}(\mathbf{x})|\Omega\rangle, \tag{1}$$

and fluctuations of the Heisenberg field around this mean value are described by

$$\delta\hat{\psi}(\mathbf{x}) \;=\; \hat{\psi}(\mathbf{x}) - \Phi(\mathbf{x}). \tag{2}$$

The fact that the correlators

$$\langle\Omega|\delta\hat{\psi}^{\dagger}(\mathbf{x})\,\delta\hat{\psi}(\mathbf{y})|\Omega\rangle \;\neq\; 0 \tag{3}$$

even at zero temperature expresses the *quantum depletion*: a fraction of the quanta is not in the condensate mode, but these depleted quanta are still part of the same ground-state distribution. In this sense, we shall associate the superfluid component with the ground state itself, consisting of the condensate together with its quantum depletion.

Quasiparticles are then defined as small-amplitude normal-mode excitations above this ground state [5]. Linearizing the dynamics around $|\Omega\rangle$ and diagonalizing the quadratic Hamiltonian one introduces operators $\hat{\alpha}_k$ and $\hat{\alpha}_k^{\dagger}$ such that, to leading order,

$$\hat{H} \;\simeq\; E_{\Omega} \;+\; \sum_k \varepsilon_k\,\hat{\alpha}_k^{\dagger}\hat{\alpha}_k, \tag{4}$$

so that $\hat{\alpha}_k^{\dagger}|\Omega\rangle$ represents a single excitation with energy ε_k above the ground state. The corresponding quasiparticle number eigenstates $|\{n_k\}\rangle$ satisfy

$$\hat{\alpha}_k^{\dagger}\hat{\alpha}_k\,|\{n_k\}\rangle \;=\; n_k\,|\{n_k\}\rangle, \quad E_{\{n_k\}} \;=\; E_{\Omega} + \sum_k \varepsilon_k n_k, \tag{5}$$

so that a whole family of excited many-body states is generated by populating the quasiparticle modes. On length and timescales larger than the *decoherence scales* [6], the many-body field can be described in terms of such quasiparticle (QP) excitations of the broken-symmetry ground state. When these quasiparticle modes are significantly populated and approximately in (local) thermal equilibrium, they constitute the *normal-fluid* component, which at large scales exhibits a classical fluid-dynamical phenomenology, while the superfluid component remains associated with the ground state (condensate plus depletion) and carries the corresponding ground-state energy. It is important to note that from this viewpoint the essence of superfluidity is symmetry breaking and the associated Goldstone phase mode, which yields a potential, inviscid flow component and quantized vortices. This structure is not intrinsically tied to microscopic quantum mechanics: it arises equally from a purely classical complex-field theory (e.g., NLSE/Ginzburg–Landau) in a broken-$U(1)$ phase. Quantum mechanics enters ^{4}He primarily by providing the microscopic realization and by fixing the effective parameters (most notably the circulation quantum). More generally, in the absence of spontaneous symmetry breaking many quantum many-body systems admit a long-wavelength description by ordinary (classical-looking) hydrodynamics, whereas broken continuous symmetries add Goldstone fields and thus qualitatively new hydrodynamic sectors (superfluidity).

A key difficulty in understanding superfluid dynamics is the extensive hierarchy of spatial and temporal scales inherent in this quantum field-theoretic description. The various regimes of this hierarchy are summarized in the scale ladders of Fig. 1, which will serve as a guide for the subsequent derivations.Within the corresponding space-time ladders, one class of scales is particularly important. Above the quasiparticle relaxation scales, the quasiparticles cross over from a kinetic-theory description to a continuum mechanical one. It is useful here to stress an important difference between the broken and unbroken phases. In the unbroken case there is only the normal-fluid component, and between the quasiparticle relaxation scales and the large hydrodynamic (turbulent) scales there are no additional normal-fluid dynamical degrees of freedom. This intermediate band is a "dynamical desert" in which no new motions appear. In this situation, the separation between relaxation scales and convective scales allows one to apply a gradient

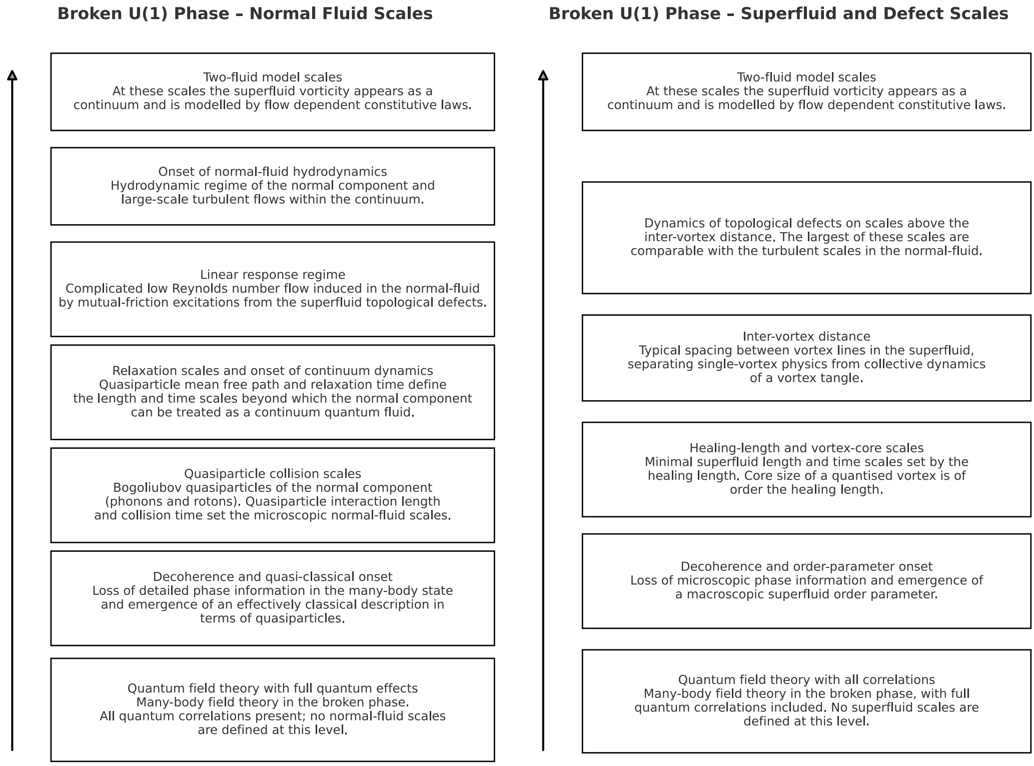

FIG. 1. Hierarchies of dynamically relevant space-timescales in the quantum field theory of a spin-0 liquid with spontaneously broken $U(1)$ symmetry. Left: the ladder of normal-fluid scales. Right: the ladder of superfluid scales. The scales grow larger as we march toward the top.

Chapman-Enskog expansion to the quantum Boltzmann/Uehling-Uhlenbeck equation, and thereby derive hydrodynamic equations for the normal-fluid, namely the Navier-Stokes equations [7,8].

In the broken phase, by contrast, the presence of superfluid topological defects (quantized vortices) populates the above mentioned *mesoscopic* desert of dynamical scales. The motion of the vortex lines and their mutual-friction coupling to the normal component excite nontrivial normal-fluid motion in the very region that would be dynamically empty in the purely normal (unbroken) phase, before both components are finally described by a coarse-grained two-fluid hydrodynamics at the largest scales.

It is important to note that, although the normal-fluid motion excited by the superfluid vortices in the mesoscopic regime is already continuum, it is not yet hydrodynamic, since these scales are not separated from the relaxation scales. Indeed, in the mesoscopic range of scales, the normal fluid is more naturally described within linear-response theory (LRT) [9]: as small perturbations around local equilibrium driven by the mutual-friction forcing. The LRT equations reduce to the linearized Navier-Stokes equation, essentially because the constitutive viscous-stress law is the same in both the hydrodynamic and LRT regimes. The difference is not the form of the constitutive relation but the range of scales and amplitudes to which it is applied. The usual hydrodynamic description is aimed at the larger, convective scales of the continuum flow, describing strongly out of equilibrium phenomena such as turbulence or shock wave propagation, whereas it does not resolve the fastest mesoscopic scales excited by the shortest Kelvin waves on the topological defects. Those fast but small-amplitude normal-fluid motions are precisely the scales where LRT is applicable.

In summary, the Navier-Stokes equation and its linearized version provide the continuum description of the normal fluid and, in principle, apply to all continuum motions (both hydrodynamic and LRT). In this sense they can describe all normal-fluid dynamics above the relaxation scales. However, at present there is no general formulation of continuum normal-fluid dynamics in the LRT regime, including the associated self-consistent interactions between the normal fluid and discrete topological defects, that is derived and employed on the same footing as the usual hydrodynamic description. Moreover, there is no framework that couples the LRT and hydrodynamic regimes into a unified analytical and computational scheme, derived from first principles, that can accurately resolve all continuum normal-fluid scales simultaneously, together with the corresponding motion of the topological defects.

Such a framework would be highly desirable. Many helium-4 phenomena take place primarily in the LRT regime [10] and, moreover, the description of superfluid turbulence requires input from the LRT scales into the hydrodynamic range. A more accurate—yet computationally feasible—prediction of the two-fluid regime would follow from a complete set of continuum equations that consistently covers both LRT and hydrodynamic scales in the normal fluid, together with their interscale coupling, and includes the self-consistent motion of the superfluid vortices.

Previous works on superfluid dynamics [11–17] have made significant advances in the understanding of these intriguing phenomena. Historically, the line of ideas runs from Tisza's and Landau's concept of the two-fluid model, and London's connection of Bose–Einstein condensation with superfluidity, to the superfluid vortices of Feynman and Onsager, and the two-fluid hydrodynamics of Hall, Vinen, Bekharevich, Khalatnikov, and Schwarz. Schwarz, in particular, pioneered a vortex-dynamical reformulation of the superfluid flow within the Hall-Vinen-Bekharevich-Khalatnikov framework, rewriting the coarse-grained mutual-friction coupling in filament variables while treating the normal-fluid component kinematically. Following Schwarz, subsequent works introduced more fully coupled hybrid descriptions, with vortex-dynamical representation of superfluid vorticity and a continuum normal-fluid.

It is important to note that, in these hybrid models, the vortices do not correspond to actual topological defects of the condensate. Since they use flow-dependent HVBK mutual-friction coefficients, the filaments should rather be viewed as filamentary excitations of a coarse-grained continuous vorticity field (cf. Fig. 1). As a result, the solutions are essentially bound to reproduce the HVBK phenomenology, in the same way that vortex-filament methods in the Navier-Stokes equation restate its physics in vorticity space. This is a serious limitation, since HVBK is an effective field theory that depends on strong assumptions about the organization of the network of topological defects, whereas this organization is precisely one of the features that a more fundamental theory ought to predict [18]. It should also be kept in mind that the HVBK equations are most naturally applicable in flows with sufficient local vortex polarization (e.g., rotating flows), whereas in fully developed three-dimensional vortex-tangle turbulence the closure problem becomes substantially more delicate [19,20].

Because of the above reasons, superfluid hydrodynamics as a discrete topological defects theory (DTDT) was proposed in Ref. [21]. Due to their discrete nature, the effects of the defects on the normal fluid can only be defined in a distributional sense, through concentrated forces acting along the defect lines. Moreover, the mutual-friction forces on the defects can be described via microcontinuum-flow interactions between the defects and the quasiparticle-dominated normal fluid in the linear-response regime discussed above. Such descriptions require only the material parameters of the fluid as input and therefore could be used as a basis for a more general theory of superfluid dynamics.

Another recent fully coupled filament/normal-fluid formulation is the model of Galantucci *et al.* [22]. In their formulation, two distinct conceptual steps occur. First, on the superfluid side, delta-supported HVBK vorticity is treated as actual quantized vortex defects carrying the quantum of circulation. However, such a microscopic defect interpretation cannot be deduced from a coarse-grained HVBK closure, because the logical direction is the opposite: coarse-grained dynamics must arise from microscopic defect dynamics, not vice versa. Second, on the normal-fluid side, an HVBK-type coarse-grained normal-fluid velocity is then used as input to that individual-defect dynamics. The difficulty here is not that low-Reynolds-number microhydrodynamics is ignored, but that the normal-fluid velocity entering such a local description should be the appropriate undisturbed flow field at the defect scale. In a turbulent superfluid, however, an HVBK normal-fluid velocity is, in general, a coarse-grained quantity and may therefore be overly averaged to serve as that undisturbed field. Thus, the final construction does not provide a single-level microscopic/discrete-defect theory, even though its operational algorithm ends up close in spirit to the earlier Kivotides-type continuum-normal-fluid / filament coupling. The present formulation was introduced precisely to avoid that mixed-level construction by starting directly from discrete topological defects and then incorporating the defect-induced microhydrodynamics explicitly.

Although consistent, the DTDT is incomplete, because it neglects the linear-response flow fields that couple defects and normal fluid *at continuum scales too small to be captured by the numerical resolution*. As a result, the formulation does not take into account the full details of the defect-normal-fluid coupling and can at best be considered a reasonable, but not complete, resolution of the superfluid dynamics problem. In particular, when a turbulent calculation drives the network of topological defects to become denser and denser, the resolution of the normal fluid field eventually becomes insufficient to represent the small-scale LRT flows induced by mutual friction, and thus cannot accurately account for the impact of these motions on the turbulent structure of the normal fluid. For these reasons, we refer to this theory as *bare* DTDT in what follows.

In this work we remedy the deficiencies of bare DTDT by explicitly resolving the linear-response normal-fluid motions and their coupling to the superfluid defects. We propose a superfluid dynamics framework that resolves, in a computationally practical way, all continuum motions of the normal fluid above the relaxation scales and the associated wave-like excitations supported by the superfluid vortices. In the process we also uncover an additional stress, which originates in the LRT regime but directly affects the turbulence structure at hydrodynamic scales.

The proposed formulation of finite-temperature superfluid turbulence dynamics is asymptotically exact, because it exploits the scale separation inherent in the action of mutual friction. Mutual friction is generated at the vortex-core scale, of order the healing length, which is far smaller than the hydrodynamic turbulence length scales [23–25]. As a result, the normal-fluid response to this core-local forcing is rapidly relaxing and effectively inertia-free from the macroscopic viewpoint; in this overdamped limit the microcontinuum LRT dynamics reduce to a Stokes-type description. On this basis we couple, in an exact manner, the LRT motions to the hydrodynamic motions. The resulting framework applies to arbitrary superfluid flows and boundary conditions and requires only material properties as input.

The paper is organized as follows. Section II reviews the bare DTDT formulation and establishes its well-posedness as an effective field theory. Section III develops the superfluid vortex-dynamics formulation, incorporating the full linear-response/hydrodynamic-interactions contribution to the mutual-friction force levels and the resulting defect velocities. In Sec. IV we apply these equations to canonical superfluid vortex-dynamics problems in the linear-response regime and obtain analytic solutions. Section V derives a purely hydrodynamic description of normal-fluid dynamics by projecting the linear-response effects onto hydrodynamic scales, which reveals a new hydrodynamic subgrid stress of linear-response origin. It also indicates a detailed computational algorithm for the implementation of the formalism. Section VI includes a summary and a few concluding remarks that help understand the potential of the proposed framework better. Finally, in two Appendixes, we describe the evaluation of the LRT induced subgrid stress, and scale the coupled normal-fluid topological-defects system.

II. SUPERFLUID DYNAMICS WITH DISCRETE TOPOLOGICAL DEFECTS: FREELY DRAINING THEORY

Here we revisit the DTDT formulation of superfluid dynamics from the viewpoint of the present contribution. In general, a superfluid supports both potential-flow patterns and topological defects.

To focus on the key interactions between defects and the normal fluid, we shall assume here that all superfluid motion is vortex driven. Potential-flow contributions can be added to the final equations by superposition, if required.

A. Superfluid vortex dynamics

We denote by ξ the arclength parameter along a superfluid vortex line, by α_0 the vortex-core radius (which varies only mildly with temperature around $\alpha_0 \approx 10^{-8}$ cm), by ρ_s and ρ_n the superfluid and normal-fluid mass densities, and by ρ_e the effective vortex mass per unit length. The symbol ν denotes the kinematic viscosity of the normal fluid, and κ the quantum of circulation. We introduce the mutual-friction coupling viscosity $\nu_c \equiv D_\perp/\rho_n$, for which $\nu_c/\nu = 8\pi/[\ln(\delta\ell/\alpha_0) + 0.5]$, and we denote by $D_\parallel$ and $D_\perp$ the longitudinal and transverse mutual-friction drag coefficients, respectively, with $D_\perp = 8\pi\rho_n\nu/[\ln(\delta\ell/\alpha_0) + 0.5]$ and $D_\parallel = 4\pi\rho_n\nu/[\ln(\delta\ell/\alpha_0) - 0.72]$ [21,26]. Notably, ν_c/ν is $O(1)$ over a wide range of $\delta\ell/\alpha_0$ values. It is important to note that, in bare (freely draining) DTDT, the coefficients $D_\perp$ and $D_\parallel$ are the standard resistive-force/slender-body coefficients for a straight vortex in an effectively unbounded viscous fluid (free-space Stokes flow), i.e., the classical local drag laws with the usual logarithmic dependence on the chosen outer cutoff, $\delta\ell$. This bare closure is isotropic in the plane normal to the vortex-segment tangent and therefore has only the $\parallel / \perp$ structure. In the LRT theory developed here, the included hydrodynamic interactions take into account periodic and wall boundary conditions. In the periodic case, one can keep $D_\perp$ and $D_\parallel$ in the equations by ensuring that their periodic-domain values are used. In wall boundaries, and taking into account that the segments are discretization elements, hence anisotropic effects are localized very close to the boundaries, we shall keep the $\parallel / \perp$ structure and deduce $D \perp$ from the isotropization of the self-block of the full mobility. We shall be more explicit below, when the actual mathematical details of the approach are discussed.

Here $\delta\ell$ is at most equal to half of the wavelength of the smallest physically possible (i.e., undamped by mutual friction) Kelvin waves along the vortices, as indicated by Samuels and Kivotides [27], and in numerical calculations it is chosen to be the grid spacing along the topological defects. Samuels and Kivotides derived the following two relations that specify the wavelength $\ell_{\rm sd}$ of the smallest undamped Kelvin waves in homogeneous, isotropic turbulence ($\delta\ell \leqslant 0.5\ell_{\rm sd}$)

$$\frac{\ell_{\rm sd}}{\eta} = \frac{1}{2}D^{1/4}\ln\left(\frac{\ell_{\rm sd}}{2\pi\alpha_0}\right)\left(\frac{\kappa}{\nu}\right)\mathrm{Re}^{-1/4},$$

where $\eta = (\nu^3/\varepsilon)^{1/4}$ is the Kolmogorov length scale of the normal-fluid turbulence, with ε the normal-fluid kinetic-energy dissipation rate per unit mass, $\mathrm{Re} = \ell_0 u'/\nu$ is the Reynolds number of turbulence in the normal fluid, ℓ_0 is the scale of the largest normal-fluid eddies, u' is the root-mean-square amplitude of the normal-fluid velocity fluctuations, and

$$\ell_{\rm sd} = \frac{\kappa}{2u'}\ln\left(\frac{\ell_{\rm sd}}{2\pi\alpha_0}\right).$$

Noting that $\ln(\ell_{\rm sd}/2\pi\alpha_0) \approx 10$ and $\kappa/\nu \approx 1 - 10$ over a wide range of length scales and temperatures, and that the Kolmogorov scaling constant D is $O(1)$, we find that $\ell_{\rm sd}$ is smaller than η but remains within an order of magnitude of it for a broad range of Reynolds numbers, $10^2 < \mathrm{Re} < 10^{11}$ [27]. Nevertheless, increasing the spatial resolution of a turbulent simulation by one order of magnitude increases the total number of grid points by a factor of 10^3, which makes the direct resolution of normal-fluid motions at the $\ell_{\rm sd}$ scales (the LRT microflows discussed above) impractical.

The developments in this paper allow one to compute superfluid turbulence using standard η-resolving computational grids, while simultaneously evaluating the subgrid LRT flows and incorporating their effects on *both* the hydrodynamic turbulent scales and the motion of the topological defects. Remarkably, the second of the Samuels-Kivotides relations implies that we need to go to exotic turbulence intensities of the order of 10^3 m s^{-1} to have the $\ell_{\rm sd}$ scale approach within an order of magnitude the core size α_0. Hence, for the vast majority of physical flows, $\delta\ell \gg \alpha_0$, and both $D_\perp$ and $D_\parallel$ are positive.

With the exception of $\delta\ell$, all of the above quantities are material parameters. Using these symbols, we define the key dynamical field variables in the theory,

$$\mathbf{X}(\xi, t): \text{ vortex-line position,}$$

$$\mathbf{t}(\xi, t) = \frac{\partial_\xi \mathbf{X}}{|\partial_\xi \mathbf{X}|}: \text{ unit tangent,}$$

$$\mathbf{v}_L(\xi, t) = \partial_t \mathbf{X}: \text{ vortex-line velocity,}$$

$$\mathbf{v}_n(\mathbf{x}, t): \text{ normal-fluid velocity field,}$$

$$\mathbf{v}_s(\mathbf{x}, t): \text{ superfluid velocity field,}$$

$$p(\mathbf{x}, t): \text{ normal-fluid pressure field.}$$

The defect dynamics are driven by forces which are well grounded in both theoretical [28] and experimental [5] results. As explained below, these forces are the foundation of all continuum superfluid turbulence theory. By using the symbols $\mathbf{f}_i$ for inertial defect force, $\mathbf{f}_M$ for the Magnus force, $\mathbf{f}_I$ for the Iordanskii force (a special instance of the Aharonov-Bohm effect), $\mathbf{f}_\parallel$ for the longitudinal mutual-friction force, and $\mathbf{f}_\perp$ for the transverse mutual-friction force, we can write an equation for the balance of forces *per unit length* along the superfluid vortices:

$$\mathbf{f}_i + \mathbf{f}_M + \mathbf{f}_I + \mathbf{f}_\parallel + \mathbf{f}_\perp = \mathbf{0}, \tag{6}$$

$$\mathbf{f}_\mathrm{i} = \rho_\mathrm{e} \frac{\mathrm{d}\mathbf{v}_L}{\mathrm{d}t}, \tag{7}$$

$$\mathbf{f}_M = -\rho_s \kappa\, \mathbf{t} \times (\mathbf{v}_L - \mathbf{v}_s), \tag{8}$$

$$\mathbf{f}_I = -\rho_n \kappa\, \mathbf{t} \times (\mathbf{v}_L - \mathbf{v}_n), \tag{9}$$

$$\mathbf{f}_\parallel = -D_\parallel\, \mathbf{t}\, [\mathbf{t} \cdot (\mathbf{v}_L - \mathbf{v}_n)], \tag{10}$$

$$\mathbf{f}_\perp = -D_\perp\, \mathbf{t} \times \{\mathbf{t} \times (\mathbf{v}_L - \mathbf{v}_n)\}, \tag{11}$$

and in compact form,

$$\rho_\mathrm{e} \frac{\mathrm{d}\mathbf{v}_L}{\mathrm{d}t} - \rho_s \kappa\, \mathbf{t} \times (\mathbf{v}_L - \mathbf{v}_s) - \rho_n \kappa\, \mathbf{t} \times (\mathbf{v}_L - \mathbf{v}_n) - D_\parallel\, \mathbf{t}\, [\mathbf{t} \cdot (\mathbf{v}_L - \mathbf{v}_n)] \\ - D_\perp\, \mathbf{t} \times \{\mathbf{t} \times (\mathbf{v}_L - \mathbf{v}_n)\} = \mathbf{0}. \tag{12}$$

It is important to stress that the vortex-line equation encodes momentum changes in the fluid, but it does so not in the *material, field-theoretic* description, rather on the moduli space $\mathcal{M}$ whose elements are the collective coordinates of the superfluid vortex filaments. In this reduced description, the momentum change associated with superfluid inertia and pressure has already been projected onto the vortex centerlines and appears as the Magnus force.

Baym and Chandler [29] showed that, in addition to this gyroscopic Magnus contribution, there is also an "inertial" term in the vortex dynamics associated with the mass of superfluid trapped by the moving core. The corresponding effective line mass density can be estimated as $\rho_\mathrm{e} \sim \rho_s a_0^2$, which for helium II yields $\rho_\mathrm{e} \sim 10^{-20}$ kg/cm, an extremely small value compared to the magnitudes of the other forces. On the turbulent timescales of interest here the vortex dynamics are therefore effectively Aristotelian rather than Galilean: the vortex velocities adjust quasi-instantaneously to the surrounding turbulent velocity fields. This is why DTDT neglects the inertial term and solves the defect dynamics in the *overdamped* (massless-core) regime. This choice has important consequences, since it implies that (in the Aristotelian, massless-core regime) the longitudinal component of the mutual-friction force vanishes. Indeed, the line-force balance and the local geometry enforce

$$\mathbf{t} \cdot (\mathbf{v}_L - \mathbf{v}_n) = 0,$$

so only the transverse component of mutual friction survives.

We also recall that the Iordanskii force is not dissipative, despite being grouped under the heading of mutual friction: it is a reactive, transverse force rather than a viscous drag. It is important to observe that in DTDT the same mutual-friction force densities are inserted both in the superfluid vortex-dynamics equation and in the normal-fluid *material momentum* equation. At first sight this may look conceptually different from the Magnus case, where the functional form of the convection and pressure terms in the superfluid momentum equation is quite different from the Magnus force obtained after projection onto the vortex centerlines. The reason is that the mutual-friction forces are defined from the outset on the collective vortex coordinates themselves [30], so no further projection onto the moduli space $\mathcal{M}$ is required: they are already line-level objects.

Moreover, we shall now show that the two sets of forces—those acting on the normal fluid and those acting on the superfluid vortices—can be obtained from the same Rayleigh dissipation functional and conservative action. This derivation demonstrates that the mutual-friction terms in the normal-fluid and vortex-dynamics equations are two representations of a single normal-fluid-superfluid coupling and thus further supports the internal consistency of DTDT.

B. Coupling forces as generated line-supported distributions

The conservative vortex dynamics (Magnus force) and the conservative normal-fluid dynamics (Navier-Stokes) admit standard variational formulations. The nontrivial structure in any discrete-defect theory is the *defect-normal-fluid coupling*. To place the theory on solid ground, we start from the well-established expressions for the forces acting on the superfluid vortices and then construct a dissipative Rayleigh functional [31,32] and a virtual-power generator [33] such that, upon variation with respect to the superfluid variables, they reproduce the standard mutual-friction and Iordanskii forces on the superfluid vortices. The corresponding forces acting on the normal fluid are then obtained by varying the same functionals with respect to the normal-fluid variables. We show below that this procedure reproduces exactly the equations employed in the bare DTDT formulation; in particular, the employed normal-fluid and superfluid couplings are consistently generated by a single functional object.

1. Mutual-friction forces from a single dissipation potential

Dissipation due to mutual friction is encoded by a dissipation potential (Onsager/Rayleigh functional) constructed from the slip

$$\mathbf{u}(\xi, t) := \mathbf{v}_L(\xi, t) - \mathbf{v}_n(\mathbf{X}(\xi, t), t). \tag{13}$$

Rayleigh functional. We postulate

$$\boxed{R_{\mathrm{mf}}[\mathbf{v}_L, \mathbf{v}_n; \mathbf{X}] = \frac{1}{2} \int_L d\xi \; (D_\parallel \, [\mathbf{t} \cdot \mathbf{u}]^2 + D_\perp \, |\mathbf{t} \times \mathbf{u}|^2).} \tag{14}$$

Note that since this is a theory about normal-fluid and topological defects, it is $\mathbf{v}_L$ which is the relevant variable in R_{mf}.

Rayleigh variation (fixed configuration). In the Rayleigh construction we vary generalized velocities at fixed configuration,

$$\delta \mathbf{X}(\xi, t) = \mathbf{0} \quad \Rightarrow \quad \delta \mathbf{t}(\xi, t) = \mathbf{0}. \tag{15}$$

Therefore, from Eq. (13),

$$\boxed{\delta \mathbf{u}(\xi, t) = \delta \mathbf{v}_L(\xi, t) - \delta \mathbf{v}_n(\mathbf{X}(\xi, t), t).} \tag{16}$$

Let the integrand be

$$r(\mathbf{u};\mathbf{t}) := \frac{1}{2}(D_{\parallel}\,(\mathbf{t}\cdot\mathbf{u})^2 + D_{\perp}\,|\mathbf{t}\times\mathbf{u}|^2), \quad R_{\mathrm{mf}} = \int_L r\,d\xi. \tag{17}$$

Since $\delta\mathbf{t} = 0$, the first variation of r is

$$\begin{aligned}\delta r &= \tfrac{1}{2}(D_{\parallel}\,\delta[(\mathbf{t}\cdot\mathbf{u})^2] + D_{\perp}\,\delta[|\mathbf{t}\times\mathbf{u}|^2])\\ &= \tfrac{1}{2}(D_{\parallel}\,2(\mathbf{t}\cdot\mathbf{u})(\mathbf{t}\cdot\delta\mathbf{u}) + D_{\perp}\,2(\mathbf{t}\times\mathbf{u})\cdot(\mathbf{t}\times\delta\mathbf{u}))\\ &= D_{\parallel}(\mathbf{t}\cdot\mathbf{u})(\mathbf{t}\cdot\delta\mathbf{u}) + D_{\perp}(\mathbf{t}\times\mathbf{u})\cdot(\mathbf{t}\times\delta\mathbf{u}).\end{aligned} \tag{18}$$

Use the identity (valid for any vectors $\mathbf{a}$, $\mathbf{b}$ and unit $\mathbf{t}$)

$$(\mathbf{t}\times\mathbf{a})\cdot(\mathbf{t}\times\mathbf{b}) = \mathbf{a}\cdot\mathbf{b} - (\mathbf{t}\cdot\mathbf{a})(\mathbf{t}\cdot\mathbf{b}), \tag{19}$$

to rewrite the second term in Eq. (18):

$$(\mathbf{t}\times\mathbf{u})\cdot(\mathbf{t}\times\delta\mathbf{u}) = \mathbf{u}\cdot\delta\mathbf{u} - (\mathbf{t}\cdot\mathbf{u})(\mathbf{t}\cdot\delta\mathbf{u}). \tag{20}$$

Substituting Eq. (20) into Eq. (18) gives

$$\begin{aligned}\delta r &= D_{\parallel}(\mathbf{t}\cdot\mathbf{u})(\mathbf{t}\cdot\delta\mathbf{u}) + D_{\perp}(\mathbf{u}\cdot\delta\mathbf{u} - (\mathbf{t}\cdot\mathbf{u})(\mathbf{t}\cdot\delta\mathbf{u}))\\ &= D_{\perp}\,\mathbf{u}\cdot\delta\mathbf{u} + (D_{\parallel} - D_{\perp})(\mathbf{t}\cdot\mathbf{u})(\mathbf{t}\cdot\delta\mathbf{u})\\ &= [D_{\perp}\,\mathbf{u} + (D_{\parallel} - D_{\perp})(\mathbf{t}\cdot\mathbf{u})\,\mathbf{t}]\cdot\delta\mathbf{u}.\end{aligned} \tag{21}$$

Hence, using the fact that $\mathbf{t}$ is a unit vector, the vector conjugate to the slip vector is

$$\boxed{\frac{\partial r}{\partial\mathbf{u}} = D_{\perp}\,\mathbf{u} + (D_{\parallel} - D_{\perp})(\mathbf{t}\cdot\mathbf{u})\,\mathbf{t} = D_{\parallel}\mathbf{t}[\mathbf{t}\cdot\mathbf{u}] - D_{\perp}\mathbf{t}\times\{\mathbf{t}\times\mathbf{u}\}.} \tag{22}$$

From $R_{\mathrm{mf}} = \int_L r\,d\xi$ and Eq. (21),

$$\delta R_{\mathrm{mf}} = \int_L d\xi\;\delta r = \int_L d\xi\;\frac{\partial r}{\partial\mathbf{u}}(\xi,t)\cdot\delta\mathbf{u}(\xi,t). \tag{23}$$

Define

$$\mathbf{f}_{\mathrm{mf}}(\xi,t) := \frac{\partial r}{\partial\mathbf{u}}(\xi,t), \tag{24}$$

so that Eq. (23) becomes

$$\delta R_{\mathrm{mf}} = \int_L d\xi\;\mathbf{f}_{\mathrm{mf}}(\xi,t)\cdot\delta\mathbf{u}(\xi,t). \tag{25}$$

Using Eq. (16) we obtain the split

$$\boxed{\delta R_{\mathrm{mf}} = \int_L d\xi\;\mathbf{f}_{\mathrm{mf}}(\xi,t)\cdot\delta\mathbf{v}_L(\xi,t) - \int_L d\xi\;\mathbf{f}_{\mathrm{mf}}(\xi,t)\cdot\delta\mathbf{v}_n(\mathbf{X}(\xi,t),t).} \tag{26}$$

Using the identity

$$\delta\mathbf{v}_n(\mathbf{X}(\xi,t),t) = \int_\Omega \delta\mathbf{v}_n(\mathbf{x},t)\,\delta^{(3)}(\mathbf{x} - \mathbf{X}(\xi,t))\,d^3x, \tag{27}$$

where Ω is the volume of the fluid domain, and exchanging the order of integration yields

$$\delta R_{\mathrm{mf}} = \int_L d\xi\ \mathbf{f}_{\mathrm{mf}}(\xi,t)\cdot\delta\mathbf{v}_L(\xi,t) - \int_\Omega \delta\mathbf{v}_n(\mathbf{x},t)\cdot\left[\int_L d\xi\ \mathbf{f}_{\mathrm{mf}}(\xi,t)\,\delta^{(3)}(\mathbf{x}-\mathbf{X}(\xi,t))\right]d^3x. \quad (28)$$

In the Rayleigh–Lagrange framework the dissipation potential R generates *dissipative generalized forces* by

$$\boxed{\mathbf{F}^{(\mathrm{diss})} = -\frac{\delta R}{\delta\mathbf{V}},} \quad (29)$$

where $\mathbf{V}$ denotes the corresponding generalized velocity (here, field or line velocity). Thus, from Eqs. (26)–(28), the mutual-friction force per unit ξ exerted on the filament is equal to $-\mathbf{f}_{\mathrm{mf}}(\xi,t)$, and the corresponding body-force density per unit mass in the normal-fluid equation is the equal-and-opposite term obtained from the $-\delta R/\delta\mathbf{v}_n$ variation. Note that these results are consistent with the force signs in our previously mentioned superfluid vortex dynamics equation (6) and the DTDT formulation of normal-fluid dynamics. Remarkably, in the Aristotelian setting adopted in this work (lemmas imply $\mathbf{t}\cdot\mathbf{v}_L = 0$ and $\mathbf{t}\cdot\mathbf{v}_n(\mathbf{X},t) = 0$), the longitudinal mutual-friction contribution to the Navier-Stokes equation vanishes.

Thermodynamic plausibility. We need to verify that the mutual friction force is dissipative, removing kinetic energy from the system. Indeed, for fixed $\mathbf{t}(\xi,t)$ the integrand in Eq. (17) is a quadratic form in the slip $\mathbf{u}$ and may be written as

$$r(\mathbf{u};\mathbf{t}) = \tfrac{1}{2}\,\mathbf{u}\cdot\mathsf{D}(\mathbf{t})\,\mathbf{u}, \quad \mathsf{D}(\mathbf{t}) = D_\parallel\,(\mathbf{t}\otimes\mathbf{t}) + D_\perp\,(\mathsf{I}-\mathbf{t}\otimes\mathbf{t}), \quad (30)$$

so that $R_{\mathrm{mf}} = \int_L r\,d\xi$. The Rayleigh drag per unit ξ is

$$-\frac{\partial r}{\partial\mathbf{u}}(\xi,t) = -\mathbf{f}_{mf}(\xi,t) = -\,\mathsf{D}(\mathbf{t}(\xi,t))\,\mathbf{u}(\xi,t). \quad (31)$$

Therefore, the instantaneous dissipated power is

$$\mathcal{P}_{\mathrm{diss}} = -\int_L \mathbf{f}_{mf}\cdot\mathbf{u}\,d\xi = -\int_L \mathbf{u}\cdot\mathsf{D}(\mathbf{t})\,\mathbf{u}\,d\xi = -2\int_L r\,d\xi = \boxed{-\,2R_{\mathrm{mf}}}. \quad (32)$$

Consequently, the net internal mutual friction power on the coupled system is equal to

$$-\int_L d\xi\ (D_\parallel\,[\mathbf{t}\cdot\mathbf{u}]^2 + D_\perp\,|\mathbf{t}\times\mathbf{u}|^2) \leqslant 0, \quad (33)$$

hence, since (as discussed above) both $D_\parallel$ and $D_\perp$ are positive, the mutual friction force is strictly dissipative.

Incompressibility and the role of the pressure. The line-supported forcing density that appears in the normal-fluid momentum equation need not be divergence-free (indeed it is a distribution supported on $\mathbf{x} = \mathbf{X}(\xi,t)$). In the incompressible normal-fluid system,

$$\nabla\cdot\mathbf{v}_n = 0, \quad (34)$$

and the "pressure" p is a Lagrange multiplier that enforces this constraint. Thus, one inserts the forcing term as obtained from the variation, and p is determined so that $\nabla\cdot\mathbf{v}_n$ remains zero. Equivalently, taking the divergence of the momentum equation yields the usual Poisson problem for pressure (with boundary conditions consistent with the normal-fluid solver), in which the source term contains (an extra when compared with standard Navier-Stokes dynamics) $\nabla\cdot\mathbf{f}$ term. This matches exactly the numerical method employed in Ref. [21] for solving the formal system.

2. Iordanskii coupling from a virtual-power functional

We introduce the normal-fluid restriction $\mathbf{w}(\xi,t) := \mathbf{v}_n(\mathbf{X}(\xi,t),t)$, so that slip $\mathbf{u}$ becomes $\mathbf{u} := \mathbf{v}_L - \mathbf{w}$.

For arbitrary virtual velocities $\boldsymbol{\eta}_L(\xi)$ and $\boldsymbol{\eta}_w(\xi)$ on L, we postulate the internal virtual-power functional

$$\boxed{\mathcal{P}_I[\boldsymbol{\eta}_L, \boldsymbol{\eta}_w] := -\int_L d\xi\ \rho_n\kappa\ [\mathbf{t}(\xi,t)\times\mathbf{u}(\xi,t)]\cdot(\boldsymbol{\eta}_L(\xi)-\boldsymbol{\eta}_w(\xi)).} \tag{35}$$

Define the line forces as the functional derivatives with respect to the virtual velocities, i.e., the coefficients in

$$\delta\mathcal{P}_I = \int_L d\xi\ \mathbf{f}_I^{\mathrm{SF}}(\xi,t)\cdot\delta\boldsymbol{\eta}_L(\xi) + \int_L d\xi\ \mathbf{f}_I^{\mathrm{NF}}(\xi,t)\cdot\delta\boldsymbol{\eta}_w(\xi). \tag{36}$$

Since Eq. (35) is linear in $(\boldsymbol{\eta}_L, \boldsymbol{\eta}_w)$, this gives

$$\boxed{\mathbf{f}_I^{\mathrm{SF}}(\xi,t) = -\rho_n\kappa\ \mathbf{t}(\xi,t)\times\mathbf{u}(\xi,t), \quad \mathbf{f}_I^{\mathrm{NF}}(\xi,t) = \rho_n\kappa\ \mathbf{t}(\xi,t)\times\mathbf{u}(\xi,t).} \tag{37}$$

For any divergence-free Eulerian test field $\boldsymbol{\eta}_n(\mathbf{x})$, $\boldsymbol{\eta}_w(\xi) = \boldsymbol{\eta}_n(\mathbf{X}(\xi,t)) = \int_\Omega \boldsymbol{\eta}_n(\mathbf{x})\delta^{(3)}(\mathbf{x}-\mathbf{X})\,d^3x$, where Ω is the domain occupied by the superfluid. Hence, the Eulerian body-force density is defined up to a gauge term $\nabla\pi_I(\mathbf{x},t)$

$$\boxed{\int_L d\xi\ \mathbf{f}_I^{\mathrm{NF}}(\xi,t)\,\delta^{(3)}(\mathbf{x}-\mathbf{X}(\xi,t))\ +\ \nabla\pi_I(\mathbf{x},t),} \tag{38}$$

where, similar to the mutual-friction force case, $\nabla\pi_I$ can be absorbed into the incompressibility pressure.

The coupling is nondissipative, since the total Iordanskii force power is

$$\int_L d\xi\ \mathbf{f}_I^{\mathrm{SF}}\cdot\mathbf{v_L} + \int_L d\xi\ \mathbf{f}_I^{\mathrm{NF}}\cdot\mathbf{v_n} = -\rho_n\kappa\int_L d\xi\ [\mathbf{t}\times\mathbf{u}]\cdot\mathbf{u} = 0. \tag{39}$$

C. Normal-fluid dynamics

By adding the above derived normal-fluid mutual friction and Iordanskii forces to the *hydrodynamic* Navier-Stokes equations, we confirm the bare DTDT theory

$$\nabla\cdot\mathbf{v}_n(\mathbf{x},t) = 0. \tag{40}$$

$$\begin{aligned}
&\frac{\partial\mathbf{v}_n(\mathbf{x},t)}{\partial t}\ +\ \nabla\left(\frac{p(\mathbf{x},t)}{\rho_n+\rho_s}+\frac{\mathbf{v}_n(\mathbf{x},t)\cdot\mathbf{v}_n(\mathbf{x},t)}{2}\right)\ -\ \mathbf{v}_n(\mathbf{x},t)\times(\nabla\times\mathbf{v}_n(\mathbf{x},t))\\
&\quad -\ \nu\,\nabla^2\mathbf{v}_n(\mathbf{x},t)\\
&\quad -\ \nu_c\int_L \mathrm{d}\xi\ \{\mathbf{t}(\xi,t)\times[\mathbf{t}(\xi,t)\times(\mathbf{v}_n(\mathbf{X}(\xi,t),t)-\mathbf{v}_L(\xi,t))]\}\,\delta^{(3)}(\mathbf{x}-\mathbf{X}(\xi,t))\\
&\quad -\ \kappa\int_L \mathrm{d}\xi\ [\mathbf{t}(\xi,t)\times(\mathbf{v}_n(\mathbf{X}(\xi,t),t)-\mathbf{v}_L(\xi,t))]\,\delta^{(3)}(\mathbf{x}-\mathbf{X}(\xi,t))\ =\ \mathbf{0}.
\end{aligned} \tag{41}$$

III. SUPERFLUID DYNAMICS WITH DISCRETE TOPOLOGICAL DEFECTS: HYDRODYNAMIC INTERACTIONS THEORY

Here, we move beyond bare DTDT and we introcude LRT microflows, i.e., microflow hydrodynamic interactions between topological defects. It is important to note that in doing this we keep the key assumption of the bare DTDT of treating the superfluid vortex cores as impenetrable objects to the normal-fluid. However, this is not a necessary assumption, and one can use partially penetrable models depending on the physics of the particular superfluid. The impenetrable model in the Aristotelian limit gives defect motion equations consistent with both experiment and the theoretical analysis of Thompson and Stamp [28], although the equations in the latter are derived *as a special case in the overdamped regime of the present formulation*.

We use the same symbols as before for the unit tangent $\mathbf{t}$, the line velocity $\mathbf{v}_L$, the normal-fluid velocity $\mathbf{v}_n$, and the superfluid velocity $\mathbf{v}_s$. As already mentioned, in the Aristotelian limit, the longitudinal mutual friction force (with coefficient $D_\parallel$) becomes zero, hence the local overdamped force balance of DTDT theory can be written as

$$D_\perp\, \mathbf{t} \times (\mathbf{t} \times (\mathbf{v}_L - \mathbf{v}_n)) \;+\; \rho_n\kappa\, \mathbf{t} \times (\mathbf{v}_L - \mathbf{v}_n) \;+\; \rho_s\kappa\, \mathbf{t} \times (\mathbf{v}_L - \mathbf{v}_s) \;=\; 0, \tag{42}$$

where $D_\perp$ is the transverse mutual-friction coefficient, and ρ_n, ρ_s are the normal and superfluid densities.

Before introducing hydrodynamic-interaction/LRT flow effects, we need to write DTDT in a more general form using vectors and operators. In particular, we define the transverse projector

$$\mathbf{Q} := \mathbf{I} - \mathbf{t}\mathbf{t}^\top \tag{43}$$

and the cross-product operator

$$\mathbf{K} := [\mathbf{t}\times], \quad \mathbf{K}\,\mathbf{a} = \mathbf{t} \times \mathbf{a}, \tag{44}$$

which satisfies $\mathbf{K}^2 = -\,\mathbf{Q}$ and $\mathbf{K}\mathbf{t} = \mathbf{0}$. Using the identity

$$\mathbf{t} \times (\mathbf{t} \times \mathbf{w}) = \mathbf{t}(\mathbf{t} \cdot \mathbf{w}) - \mathbf{w} = -\,\mathbf{Q}\mathbf{w}, \tag{45}$$

we can rewrite Eq. (42) in the form

$$-D_\perp\, \mathbf{Q}(\mathbf{v}_L - \mathbf{v}_n) \;+\; \rho_n\kappa\, \mathbf{K}(\mathbf{v}_L - \mathbf{v}_n) \;+\; \rho_s\kappa\, \mathbf{K}(\mathbf{v}_L - \mathbf{v}_s) \;=\; 0. \tag{46}$$

DTDT imposes the gauge $\mathbf{t} \cdot \mathbf{v}_L = 0$, and, in the Aristotelian limit, incorporates the tangential slip condition $\mathbf{t} \cdot (\mathbf{v}_L - \mathbf{v}_n) = 0$ (hence also $\mathbf{t} \cdot \mathbf{v}_n = 0$), so that the physically relevant velocities are effectively transverse. After some algebra, the local relation can be cast in the compact form

$$\mathbf{A}\,\mathbf{v}_L \;=\; \rho_s\kappa\,\mathbf{Q}\,\mathbf{v}_s \;+\; \mathbf{B}\,\mathbf{v}_n, \tag{47}$$

with

$$\mathbf{A} = a\,\mathbf{I} + b\,\mathbf{K}, \quad \mathbf{B} = \rho_n\kappa\,\mathbf{I} + b\,\mathbf{K}, \tag{48}$$

where

$$a = (\rho_s + \rho_n)\kappa, \quad b = D_\perp. \tag{49}$$

As already mentioned, the employed $\parallel$ / $\perp$ structure is exact for unbounded and periodic flows, and, a reasonable approximation in wall-bounded flows, where $D\perp$ is deduced by the isotropization of the self-block of the full mobility matrix. Errors from this approximation are confined to the self-interaction part of the mobility/resistance tensor and within layers of thickness $O(\delta\ell)$ in the vicinity of wall boundaries. Since $\delta\ell$ is a discretization length scale, these layers are very small in comparison with the typical scales in the problem.

A. Faxén relation and hydrodynamic interactions

To include linear-response flow modes via hydrodynamic interactions, we keep the local DTDT overdamped force balance unchanged, but we modify the *normal-fluid velocity entering the DTDT drag law*. Specifically, we take this normal-fluid input velocity to be the undisturbed background flow plus the Stokes disturbance produced at the segment location by the forces exerted on the normal fluid by *all other* segments. Denoting by $\bar{\mathbf{v}}_n$ the prescribed background normal flow (e.g., imposed counterflow or a coarse–grained Navier-Stokes solution), and by $\mathbf{S}_{\text{off}}$ the off-diagonal part of the Stokes Green's operator [34,35] (segment-segment couplings only), we make the replacement

$$\mathbf{v}_n \;\to\; \bar{\mathbf{v}}_n \;-\; \rho_s\kappa\,\mathbf{S}_{\text{off}}\,\mathbf{K}\,(\mathbf{v}_L - \mathbf{v}_s). \tag{50}$$

This is the superfluid analog of a Faxén-type construction [24]: the normal-fluid velocity sampled in the local drag law is augmented by the microhydrodynamic disturbance induced by nonlocal forcing. By action-reaction, the force applied *to the normal fluid* by a segment is the negative of the force applied *to the segment* by the normal fluid. In the overdamped DTDT balance the latter equals $-\mathbf{f}_M$, hence the forcing of the normal fluid is $+\mathbf{f}_M$; accordingly, the hydrodynamic-interaction correction in Eq. (50) is driven by $\mathbf{f}_M$ and involves only off-diagonal segment-segment couplings.

Substituting Eq. (50) into Eq. (47) gives

$$\begin{aligned}\mathbf{A}\,\mathbf{v}_L &= \rho_s\kappa\,\mathbf{Q}\,\mathbf{v}_s \;+\; \mathbf{B}(\bar{\mathbf{v}}_n \;-\; \rho_s\kappa\,\mathbf{S}_{\text{off}}\,\mathbf{K}\,(\mathbf{v}_L-\mathbf{v}_s))\\ &= \rho_s\kappa\,\mathbf{Q}\,\mathbf{v}_s \;+\; \mathbf{B}\,\bar{\mathbf{v}}_n \;-\; \rho_s\kappa\,\mathbf{B}\,\mathbf{S}_{\text{off}}\mathbf{K}\,\mathbf{v}_L \;+\; \rho_s\kappa\,\mathbf{B}\,\mathbf{S}_{\text{off}}\mathbf{K}\,\mathbf{v}_s.\end{aligned} \tag{51}$$

Gathering the terms proportional to $\mathbf{v}_L$ on the left-hand side yields

$$(\mathbf{A} \;+\; \rho_s\kappa\,\mathbf{B}\,\mathbf{S}_{\text{off}}\mathbf{K})\mathbf{v}_L \;=\; \rho_s\kappa\,(\mathbf{Q}+\mathbf{B}\,\mathbf{S}_{\text{off}}\mathbf{K})\mathbf{v}_s \;+\; \mathbf{B}\,\bar{\mathbf{v}}_n. \tag{52}$$

Assuming the operator in parentheses is invertible on the transverse subspace, we obtain the Brownian-dynamics-type kinematic expression

$$\boxed{\mathbf{v}_L = (\mathbf{A} \;+\; \rho_s\kappa\,\mathbf{B}\,\mathbf{S}_{\text{off}}\mathbf{K})^{-1}[\rho_s\kappa\,(\mathbf{Q}+\mathbf{B}\,\mathbf{S}_{\text{off}}\mathbf{K})\mathbf{v}_s \;+\; \mathbf{B}\,\bar{\mathbf{v}}_n].} \tag{53}$$

B. Rewriting in terms of S_{full} and $\sigma_\perp$

Numerically, it is natural to work with the full Stokes *mobility* operator $\mathbf{S}_{\text{full}}$ delivered by a P3M (particle-particle particle-mesh [36]) solver and its self-block $\boldsymbol{\Sigma}$. We split

$$\mathbf{S}_{\text{off}} = \mathbf{S}_{\text{full}} - \boldsymbol{\Sigma}. \tag{54}$$

Because the vortex line singles out the direction $\mathbf{t}$, the most general axisymmetric self-block can be written as

$$\boldsymbol{\Sigma} = \sigma_\perp\,\mathbf{Q} + \sigma_\parallel\,\mathbf{t}\mathbf{t}^\top. \tag{55}$$

However, in the vortex dynamics $\boldsymbol{\Sigma}$ always appears multiplied by $\mathbf{K}$. Using

$$\mathbf{t}\mathbf{t}^\top\mathbf{K} = \mathbf{0}, \quad \mathbf{Q}\mathbf{K} = \mathbf{K}, \tag{56}$$

we have

$$\boldsymbol{\Sigma}\,\mathbf{K} = \sigma_\perp\,\mathbf{Q}\mathbf{K} = \sigma_\perp\,\mathbf{K}. \tag{57}$$

Thus, only the transverse self-coefficient $\sigma_\perp$ enters the dynamics; the longitudinal part $\sigma_\parallel$ is dynamically irrelevant in this model.

Inserting $\mathbf{S}_{\text{off}} = \mathbf{S}_{\text{full}} - \boldsymbol{\Sigma}$ into Eq. (52), the operator on the left becomes

$$\begin{aligned}\mathbf{L} &:= \mathbf{A} + \rho_s\kappa\,\mathbf{B}\,\mathbf{S}_{\text{off}}\mathbf{K}\\ &= \mathbf{A} + \rho_s\kappa\,\mathbf{B}\,(\mathbf{S}_{\text{full}} - \boldsymbol{\Sigma})\mathbf{K}\\ &= (\mathbf{A} - \rho_s\kappa\,\mathbf{B}\,\boldsymbol{\Sigma}\mathbf{K}) \;+\; \rho_s\kappa\,\mathbf{B}\,\mathbf{S}_{\text{full}}\mathbf{K}.\end{aligned} \tag{58}$$

Using $\boldsymbol{\Sigma}\mathbf{K} = \sigma_\perp\mathbf{K}$, we define an effective local operator

$$\boxed{\mathbf{A}_{\text{eff}} := \mathbf{A} - \rho_s\kappa\,\sigma_\perp\,\mathbf{B}\,\mathbf{K},} \tag{59}$$

so that

$$\mathbf{L} = \mathbf{A}_{\text{eff}} \;+\; \rho_s\kappa\,\mathbf{B}\,\mathbf{S}_{\text{full}}\mathbf{K}. \tag{60}$$

Similarly, the right-hand side of Eq. (52) becomes

$$\begin{aligned}\mathbf{R} &:= \rho_s\kappa\,(\mathbf{Q}+\mathbf{B}\,\mathbf{S}_{\text{off}}\mathbf{K})\mathbf{v}_s \;+\; \mathbf{B}\,\bar{\mathbf{v}}_n\\ &= \rho_s\kappa\,(\mathbf{Q}+\mathbf{B}\,\mathbf{S}_{\text{full}}\mathbf{K}-\mathbf{B}\,\mathbf{\Sigma}\mathbf{K})\mathbf{v}_s \;+\; \mathbf{B}\,\bar{\mathbf{v}}_n\\ &= \rho_s\kappa\,(\mathbf{Q}+\mathbf{B}\,\mathbf{S}_{\text{full}}\mathbf{K}-\sigma_\perp\,\mathbf{B}\,\mathbf{K})\mathbf{v}_s \;+\; \mathbf{B}\,\bar{\mathbf{v}}_n.\end{aligned} \tag{61}$$

We denote this compactly as

$$\boxed{\mathbf{R}_{\text{eff}} := \rho_s\kappa\,(\mathbf{Q}+\mathbf{B}\,\mathbf{S}_{\text{full}}\mathbf{K}-\sigma_\perp\,\mathbf{B}\,\mathbf{K})\mathbf{v}_s \;+\; \mathbf{B}\,\bar{\mathbf{v}}_n.} \tag{62}$$

Putting everything together, the hydrodynamic-interaction resolved vortex kinematics can be written in the final form

$$\boxed{\mathbf{v}_L = (\mathbf{A}_{\text{eff}} \;+\; \rho_s\kappa\,\mathbf{B}\,\mathbf{S}_{\text{full}}\mathbf{K})^{-1}\mathbf{R}_{\text{eff}},} \tag{63}$$

with $\mathbf{A}_{\text{eff}}$ and $\mathbf{R}_{\text{eff}}$ given by Eqs. (59) and (62), and $\sigma_\perp$ the transverse self-term (a single scalar) associated with the chosen periodic box, P3M kernel and core model.

Isotropized self-block and definition of $\sigma_\perp$. The matrix $\mathbf{\Sigma}$ above consists of N 3×3 blocks $\mathbf{\Sigma_j}$, each corresponding to the three dimensional self-interaction of segment j with itself. In other words, multiplying $\mathbf{\Sigma_j}$ with the sum of the mutual friction and Iordanskii forces on the normal-fluid at the segment location gives the self-induced velocity of segment j. Using the vortex force balance in the Aristotelian limit, we see that this sum is equal to the Magnus force, a fact used in numerical calculations.

Because the vortex line singles out the direction $\mathbf{t}_j$, the most general *axisymmetric* 3×3 self-mobility block can be written as

$$\boxed{\mathbf{\Sigma}_j = \sigma_{\perp,j}\,\mathbf{Q}_j + \sigma_{\|,j}\,\mathbf{t}_j\mathbf{t}_j^\top, \quad \mathbf{Q}_j := \mathbf{I}-\mathbf{t}_j\mathbf{t}_j^\top.} \tag{64}$$

Here $\mathbf{Q}_j$ is the 3×3 projector onto the plane normal to $\mathbf{t}_j$ ($\mathbf{Q}_j^2 = \mathbf{Q}_j$, $\operatorname{tr}\mathbf{Q}_j = 2$).

In actual calculations, a numerical method such as P3M provides the Stokes mobility operator (and, when assembled, the full $3N\times 3N$ mobility matrix), hence in particular the diagonal self-interaction blocks $\mathbf{\Sigma}_j$. Having $\mathbf{\Sigma}_j$ available allows the computation of the isotropized transverse mobility

$$\boxed{\sigma_{\perp,j} := \tfrac{1}{2}\operatorname{tr}(\mathbf{Q}_j\,\mathbf{\Sigma}_j\,\mathbf{Q}_j),} \tag{65}$$

and the longitudinal mobility $\sigma_{\|,j} := \mathbf{t}_j^\top\mathbf{\Sigma}_j\mathbf{t}_j$. In unbounded domains, $\sigma_{\perp,j}$ reduces to the free-space (slender-body) transverse mobility; equivalently, the transverse resistance coefficient is $D_{\perp,j} = 1/\sigma_{\perp,j}$, recovering the bare DTDT coefficient. In periodic domains, transverse isotropy is exact and the above extraction is consistent with the $D_{\perp,j}$ values in the vortex dynamical equations. In wall-bounded domains, $\mathbf{\Sigma}_j$ may be weakly anisotropic in the transverse plane; then $\sigma_{\perp,j}$ is an effective isotropic average of the transverse self-mobility, while the dominant boundary physics is retained in the nonlocal hydrodynamic interactions through the off-diagonal blocks (i.e., through $\mathbf{S}_{\text{off}}$). The transverse-isotropy approximation becomes accurate as the wall distance h_j becomes large compared with the cutoff scale set by the discretization/regularization (typically comparable to δ_ℓ or the P3M smoothing kernel width).

To quantify the transverse isotropization error in wall-bounded geometries, we define the transverse self-block

$$\mathbf{\Sigma}_{\perp,j} := \mathbf{Q}_j\,\mathbf{\Sigma}_j\,\mathbf{Q}_j, \quad \sigma_{\perp,j} := \tfrac{1}{2}\operatorname{tr}(\mathbf{\Sigma}_{\perp,j}). \tag{66}$$

In the two-dimensional subspace orthogonal to $\mathbf{t}_j$, the symmetric operator $\mathbf{\Sigma}_{\perp,j}$ has two (generally distinct) eigenvalues, denoted $\lambda_{1,j} \geqslant \lambda_{2,j} \geqslant 0$. The isotropic transverse approximation replaces

$\boldsymbol{\Sigma}_{\perp,j}$ by $\sigma_{\perp,j}\mathbf{Q}_j$, i.e., by using the average eigenvalue $\sigma_{\perp,j} = (\lambda_{1,j} + \lambda_{2,j})/2$. A natural dimensionless measure of the anisotropy discarded by this isotropization is therefore the relative eigenvalue split

$$\boxed{\varepsilon_{\perp,j} := \frac{\lambda_{1,j} - \lambda_{2,j}}{\lambda_{1,j} + \lambda_{2,j}}, \quad 0 \leqslant \varepsilon_{\perp,j} < 1,} \tag{67}$$

which vanishes if and only if the transverse self-response is isotropic. In periodic (and free-space) geometries, symmetry implies $\lambda_{1,j} = \lambda_{2,j}$ (up to numerical accuracy), so $\varepsilon_{\perp,j} \approx 0$ and the isotropization is exact. In wall-bounded domains $\varepsilon_{\perp,j}$ increases as the segment approaches a boundary, reflecting the wall-induced transverse anisotropy of the local self-response. Since the self term represents a regularized near-field contribution with a cutoff set by the discretization/regularization scale, $\varepsilon_{\perp,j}$ decays with wall distance h_j and becomes small when h_j is large compared with that cutoff scale (typically comparable to the segment length or P3M smoothing kernel width), so that the isotropized coefficient $\sigma_{\perp,j}$ accurately represents the bulk self-response.

Practical evaluation of $\sigma_{\perp,j}$ when the mobility is not assembled. In many P3M implementations the $3N \times 3N$ mobility matrix is not formed explicitly; instead, the Stokes solver provides only the *action* of the mobility operator on a prescribed body-force density. The extraction of $\sigma_{\perp,j}$ nevertheless remains straightforward, because it requires only the local (self) response of the solver to a *single-segment* forcing.

Single-segment probe. Fix a segment j with midpoint $\mathbf{X}_j$ and tangent $\mathbf{t}_j$, and choose two orthonormal unit vectors $\mathbf{e}_{\perp,1}, \mathbf{e}_{\perp,2}$ spanning the plane normal to $\mathbf{t}_j$ ($\mathbf{e}_{\perp,\alpha} \cdot \mathbf{t}_j = 0$). For each $\alpha \in \{1, 2\}$, apply a *unit* line force $\mathbf{q}_j = \mathbf{e}_{\perp,\alpha}$ on segment j only (all other segment forces set to zero), solve numerically the Stokes problem with the prescribed boundary conditions, and interpolate the resulting LRT normal-fluid velocity back to the segment midpoint to obtain $\mathbf{v}_{n,j}^{(\alpha)}$. The transverse self-mobility scalar is then obtained directly by the transverse trace average (unit force),

$$\boxed{\sigma_{\perp,j} = \frac{1}{2}\sum_{\alpha=1}^{2} \mathbf{e}_{\perp,\alpha} \cdot \mathbf{v}_{n,j}^{(\alpha)}.} \tag{68}$$

If desired, the longitudinal mobility can be obtained analogously by a probe with $\mathbf{q}_j = \mathbf{t}_j$, giving $\sigma_{\parallel,j} = \mathbf{t}_j \cdot \mathbf{v}_{n,j}^{(\parallel)}$. Equation (68) is equivalent to $\sigma_{\perp,j} = \frac{1}{2}\,\mathrm{tr}(\mathbf{Q}_j\boldsymbol{\Sigma}_j\mathbf{Q}_j)$, but it does not require constructing $\boldsymbol{\Sigma}_j$ explicitly.

Periodic versus wall-bounded domains. In fully periodic domains the self-mobility is translationally invariant and (by symmetry) isotropic in the transverse plane, so a single probe evaluation yields a constant $\sigma_\perp$ that may be used for all segments. In wall-bounded domains, $\sigma_{\perp,j}$ depends on the segment position and orientation relative to the boundary (primarily through the wall distance h_j and, if needed, the angle between $\mathbf{t}_j$ and the wall normal). In practice we therefore precompute $\sigma_\perp$ by a set of single-segment probe solves performed at representative distances (and orientations, if required), store the results in a lookup table, and evaluate $\sigma_{\perp,j}$ during time stepping by interpolation in the table. This procedure retains full boundary-condition consistency because each probe solve uses the same Stokes solver and regularization as the production calculations.

IV. ANALYTICAL SOLUTIONS IN THE LINEAR-RESPONSE REGIME

To clarify the physical impact of hydrodynamic interactions on defect motion, we now present several solutions of the formal system in the purely linear-response regime. Any new effects are illustrated by comparing these full solutions with the corresponding bare DTDT solutions.

A. Two parallel straight vortices in an unbounded domain

We consider two infinite straight vortices of equal circulation κ, both aligned with the z axis,

$$\mathbf{t} = \hat{\mathbf{z}}. \tag{69}$$

Their centerline positions in the (x, y) plane are $\mathbf{X}_1(t)$ and $\mathbf{X}_2(t)$, and we define the separation vector and distance as

$$\mathbf{r}(t) = \mathbf{X}_1(t) - \mathbf{X}_2(t), \quad d(t) = \|\mathbf{r}(t)\|. \tag{70}$$

The undisturbed normal flow is taken to be zero, $\bar{\mathbf{v}}_n = \mathbf{0}$. For infinite straight vortices the self-Biot-Savart velocity on the line vanishes, so the superfluid velocity at each line is induced only by the other line.

Because $\mathbf{t}$ is fixed, it is convenient to introduce the 3D transverse projector and the cross-product operator

$$\mathbf{Q} := \mathbf{I} - \mathbf{t}\mathbf{t}^{\top} = \mathrm{diag}(1, 1, 0), \quad \mathbf{K} := [\mathbf{t}\times]. \tag{71}$$

In the present configuration all physically relevant velocities and forces are transverse, i.e., orthogonal to $\mathbf{t}$. Hence, the dynamics closes on the transverse subspace and we work with the restrictions of these operators to the (x, y) plane:

$$\mathbf{Q}_{\perp} := \mathbf{Q}\big|_{\perp} = \mathbf{I}_{\perp}, \quad \mathbf{K}_{\perp} := \mathbf{K}\big|_{\perp}, \tag{72}$$

where $\mathbf{I}_{\perp}$ is the 2×2 identity. On this subspace one has

$$\mathbf{K}_{\perp}^2 = -\mathbf{I}_{\perp}. \tag{73}$$

Accordingly, below $\mathbf{r}$, $\mathbf{v}_s$, $\mathbf{v}_L$ are understood as transverse vectors (equivalently, 2–component vectors in the (x, y) plane), and $\mathbf{K}_{\perp}$ acts as a $\pi/2$ rotation.

1. Freely draining DTDT

In the absence of hydrodynamic interactions, the normal-fluid velocity entering the drag law is the undisturbed flow field that we now is equal to zero. Hence, in our general vortex dynamics equation, we have $\mathbf{v}_n = \mathbf{0}$, and the local overdamped DTDT balance reduces (in the transverse subspace) to

$$\mathbf{A}_{\perp}\,\mathbf{v}_L = \rho_s\kappa\,\mathbf{Q}_{\perp}\,\mathbf{v}_s = \rho_s\kappa\,\mathbf{v}_s, \quad \mathbf{A}_{\perp} = a\,\mathbf{I}_{\perp} + b\,\mathbf{K}_{\perp}, \tag{74}$$

with

$$a = (\rho_s + \rho_n)\kappa, \quad b = D_{\perp}. \tag{75}$$

Using $\mathbf{K}_{\perp}^2 = -\mathbf{I}_{\perp}$, the inverse is

$$\mathbf{A}_{\perp}^{-1} = \frac{1}{a^2 + b^2}(a\,\mathbf{I}_{\perp} - b\,\mathbf{K}_{\perp}). \tag{76}$$

It is convenient to introduce

$$\alpha_1 := \rho_s\kappa\,\frac{a}{a^2 + b^2}, \quad \alpha_2 := -\,\rho_s\kappa\,\frac{b}{a^2 + b^2}, \tag{77}$$

so that

$$\mathbf{v}_L = \rho_s\kappa\,\mathbf{A}_{\perp}^{-1}\mathbf{v}_s = \alpha_1\,\mathbf{v}_s + \alpha_2\,\mathbf{K}_{\perp}\,\mathbf{v}_s. \tag{78}$$

For two parallel vortices, the Biot-Savart velocity induced at vortex 1 by vortex 2 is purely transverse, with magnitude $\kappa/(2\pi d)$ and—by choosing the vortex tangent $\mathbf{t}$ to point along the vorticity direction—direction $\mathbf{K}_\perp \mathbf{r}$:

$$\mathbf{v}_{s,1} = \frac{\kappa}{2\pi d^2}\,\mathbf{K}_\perp\,\mathbf{r}, \quad \mathbf{v}_{s,2} = -\,\frac{\kappa}{2\pi d^2}\,\mathbf{K}_\perp\,\mathbf{r}. \tag{79}$$

Therefore,

$$\mathbf{K}_\perp \mathbf{v}_{s,1} = \frac{\kappa}{2\pi d^2}\,\mathbf{K}_\perp^2 \mathbf{r} = -\,\frac{\kappa}{2\pi d^2}\,\mathbf{r}, \quad \mathbf{K}_\perp \mathbf{v}_{s,2} = -\,\frac{\kappa}{2\pi d^2}\,\mathbf{K}_\perp^2 \mathbf{r} = \frac{\kappa}{2\pi d^2}\,\mathbf{r}. \tag{80}$$

Inserting these in Eq. (78) gives

$$\mathbf{v}_{L,1} = \frac{\kappa}{2\pi d^2}(\alpha_1\,\mathbf{K}_\perp \mathbf{r} - \alpha_2\,\mathbf{r}), \quad \mathbf{v}_{L,2} = \frac{\kappa}{2\pi d^2}(-\alpha_1\,\mathbf{K}_\perp \mathbf{r} + \alpha_2\,\mathbf{r}). \tag{81}$$

The separation vector evolves according to

$$\frac{\mathrm{d}\mathbf{r}}{\mathrm{d}t} = \mathbf{v}_{L,1} - \mathbf{v}_{L,2} = \frac{\kappa}{\pi d^2}(\alpha_1\,\mathbf{K}_\perp \mathbf{r} - \alpha_2\,\mathbf{r}). \tag{82}$$

It is convenient to parametrize the relative dynamics by a radial drift rate $\gamma_r(d)$ and an angular frequency $\Omega(d)$ through

$$\frac{\mathrm{d}\mathbf{r}}{\mathrm{d}t} = -\,\gamma_r^{(0)}(d)\,\mathbf{r} + \Omega^{(0)}(d)\,\mathbf{K}_\perp \mathbf{r}, \tag{83}$$

so that $\dot{d} = -\gamma_r(d)\,d$ and $\dot{\theta} = \Omega(d)$. The superscript (0) denotes the freely draining (no–HI) limit $\mathbf{S}_{\mathrm{off}} = \mathbf{0}$; when hydrodynamic interactions are included the corresponding rates are written $\gamma_r^{(\mathrm{HI})}(d)$ and $\Omega^{(\mathrm{HI})}(d)$. Inserting the $\alpha_{1,2}$ values, we have

$$\gamma_r^{(0)}(d) = \frac{\kappa}{\pi d^2}\,\alpha_2 = -\,\frac{\rho_s \kappa^2\, b}{\pi d^2\,(a^2+b^2)}, \quad \Omega^{(0)}(d) = \frac{\kappa}{\pi d^2}\,\alpha_1 = \frac{\rho_s \kappa^2\, a}{\pi d^2\,(a^2+b^2)}. \tag{84}$$

Writing $\mathbf{r} = d\,\mathbf{e}_r$ with $\mathbf{e}_r$ a radial unit vector and $\mathbf{e}_\theta = \mathbf{K}_\perp \mathbf{e}_r$ the azimuthal unit vector, projecting Eq. (83) along $\mathbf{e}_r$ and $\mathbf{e}_\theta$ yields

$$\frac{\mathrm{d}d}{\mathrm{d}t} = -\,\gamma_r^{(0)}(d)\,d = \frac{C_r}{d}, \quad \frac{\mathrm{d}\theta}{\mathrm{d}t} = \Omega^{(0)}(d) = \frac{C_\theta}{d^2}, \tag{85}$$

with the constants

$$C_r = \frac{\rho_s \kappa^2 b}{\pi\,(a^2+b^2)}, \quad C_\theta = \frac{\rho_s \kappa^2 a}{\pi\,(a^2+b^2)}. \tag{86}$$

Integrating the first equation gives

$$\frac{\mathrm{d}}{\mathrm{d}t}\,d^2 = 2d\,\frac{\mathrm{d}d}{\mathrm{d}t} = 2C_r \quad \Rightarrow \quad d(t)^2 = d_0^2 + 2C_r t, \tag{87}$$

so that for $b > 0$ the vortices *separate* while rotating. The angular dynamics follow from

$$\frac{\mathrm{d}\theta}{\mathrm{d}t} = \frac{C_\theta}{d(t)^2} = \frac{C_\theta}{d_0^2 + 2C_r t}, \tag{88}$$

which integrates to

$$\theta(t) = \theta_0 + \frac{C_\theta}{2C_r}\ln\!\left(1 + \frac{2C_r t}{d_0^2}\right). \tag{89}$$

Since $b = D_\perp$, in the limit $b \to 0$ we have $C_r \to 0$ and the vortices undergo pure circular motion at fixed separation, as in the classical inviscid picture.

Thus, in the freely draining DTDT limit without hydrodynamic interactions, two parallel vortices form a spiralling pair: they rotate around their center of mass while *separating*, with the rates set by a and b.

2. DTDT with hydrodynamic interactions

We now include hydrodynamic interactions in the normal component and use the HI-resolved DTDT kinematics (63). For two vortex segments at separation d, the reduced two-point transverse mobility matrix can be parametrized as

$$\mathbf{S}_{\text{full}}(d) = \begin{pmatrix} \sigma_\perp \mathbf{I}_\perp & \mu_\perp(d)\mathbf{I}_\perp \\ \mu_\perp(d)\mathbf{I}_\perp & \sigma_\perp \mathbf{I}_\perp \end{pmatrix}, \tag{90}$$

where $\sigma_\perp$ is the transverse self-mobility and $\mu_\perp(d)$ is the (two-point) transverse interaction mobility.

Spectral decomposition of the 4×4 *transverse mobility and antisymmetric selection.* On the transverse plane the two-point mobility (90) is a 4×4 matrix acting on $\mathbf{F} = (\mathbf{f}_1, \mathbf{f}_2)^\top$ with $\mathbf{f}_i \in \mathbb{R}^2$. It admits the exact projector decomposition

$$\mathbf{S}_{\text{full}}(d) = \lambda_+(d)\mathbf{P}_+ + \lambda_-(d)\mathbf{P}_-, \quad \lambda_\pm(d) = \sigma_\perp \pm \mu_\perp(d), \quad \mathbf{P}_\pm = \frac{1}{2}\begin{pmatrix} \mathbf{I}_\perp & \pm\mathbf{I}_\perp \\ \pm\mathbf{I}_\perp & \mathbf{I}_\perp \end{pmatrix}. \tag{91}$$

In the present equal-circulation parallel-vortex configuration the force per unit length applied to the normal fluid [the Magnus forcing entering Eq. (63)] is antisymmetric between the two vortices, $\mathbf{f}_{M,2} = -\mathbf{f}_{M,1}$; see Eq. (95). Hence, $\mathbf{F} = (\mathbf{f}, -\mathbf{f})^\top$ and

$$\mathbf{P}_+\mathbf{F} = \mathbf{0}, \quad \mathbf{P}_-\mathbf{F} = \mathbf{F}, \tag{92}$$

so that

$$\mathbf{S}_{\text{full}}(d)\,\mathbf{F} = \lambda_-(d)\,\mathbf{F} = (\sigma_\perp - \mu_\perp(d))\,(\mathbf{f}, -\mathbf{f})^\top. \tag{93}$$

Therefore, only the antisymmetric scalar combination $\lambda_-(d) = \sigma_\perp - \mu_\perp(d)$ is sampled in the relative dynamics (the symmetric sector corresponds to common translation and cancels from $\dot{\mathbf{r}} = \mathbf{v}_{L,1} - \mathbf{v}_{L,2}$).

Reduced 2×2 *transverse system.* Restricting $\mathbf{A}$ and $\mathbf{B}$ to the transverse plane gives

$$\mathbf{A}_\perp = a\,\mathbf{I}_\perp + b\,\mathbf{K}_\perp, \quad \mathbf{B}_\perp = \rho_n\kappa\,\mathbf{I}_\perp + b\,\mathbf{K}_\perp. \tag{94}$$

In Eq. (63), the mobility $\mathbf{S}_{\text{full}}$ acts on the force per unit length applied to the normal fluid by the segment. In the Aristotelian DTDT balance this forcing is the Magnus force,

$$\mathbf{f}_M = -\rho_s\kappa\,\mathbf{K}_\perp(\mathbf{v}_L - \mathbf{v}_s), \tag{95}$$

so the HI correction involves $\mathbf{S}_{\text{full}}\mathbf{f}_M$ [as incorporated in Eq. (63)]. By exchange symmetry of two identical equal–circulation vortices, the dynamics is confined to the antisymmetric subspace, so that $\mathbf{v}_{L,2} = -\mathbf{v}_{L,1}$ (and likewise for the forcing). Substituting Eq. (90) into Eq. (63) and using the antisymmetric action (93) yields the exact reduced transverse system for $\mathbf{v}_{L,1}$:

$$(\mathbf{A}_\perp - \rho_s\kappa\,\mu_\perp(d)\,\mathbf{B}_\perp\mathbf{K}_\perp)\mathbf{v}_{L,1} = \rho_s\kappa(\mathbf{I}_\perp - \mu_\perp(d)\,\mathbf{B}_\perp\mathbf{K}_\perp)\mathbf{v}_{s,1}, \quad \mathbf{v}_{L,2} = -\mathbf{v}_{L,1}. \tag{96}$$

Using $\mathbf{B}_\perp\mathbf{K}_\perp = -b\,\mathbf{I}_\perp + \rho_n\kappa\,\mathbf{K}_\perp$, define

$$\tilde{a}(d) := a + \rho_s\kappa\,b\,\mu_\perp(d), \quad \tilde{b}(d) := b - \rho_s\rho_n\kappa^2\,\mu_\perp(d), \tag{97}$$

and

$$U(d) := 1 + b\,\mu_\perp(d), \quad V(d) := \rho_n\kappa\,\mu_\perp(d). \tag{98}$$

Then Eq. (96) becomes

$$(\tilde{a}\,\mathbf{I}_\perp + \tilde{b}\,\mathbf{K}_\perp)\mathbf{v}_{L,1} = \rho_s\kappa\,\big(U\,\mathbf{I}_\perp - V\,\mathbf{K}_\perp\big)\mathbf{v}_{s,1}, \tag{99}$$

hence

$$\mathbf{v}_{L,1} = \frac{\rho_s\kappa}{\tilde{a}(d)^2 + \tilde{b}(d)^2}[(\tilde{a}(d)U(d) - \tilde{b}(d)V(d))\mathbf{I}_\perp - (\tilde{a}(d)V(d) + \tilde{b}(d)U(d))\mathbf{K}_\perp]\mathbf{v}_{s,1}, \tag{100}$$

with $\mathbf{v}_{L,2} = -\mathbf{v}_{L,1}$.

Relative dynamics and HI-renormalized rates. For two parallel straight vortices, the Biot-Savart velocity induced at vortex 1 by vortex 2 is

$$\mathbf{v}_{s,1} = \frac{\kappa}{2\pi d^2}\mathbf{K}_\perp \mathbf{r}, \quad \mathbf{r} = \mathbf{X}_1 - \mathbf{X}_2, \quad d = \|\mathbf{r}\|. \tag{101}$$

Substituting Eq. (101) into Eq. (100) and using $\mathbf{K}_\perp^2 = -\mathbf{I}_\perp$ gives

$$\mathbf{v}_{L,1} = \frac{\rho_s\kappa^2}{2\pi d^2}\frac{1}{\tilde{a}(d)^2 + \tilde{b}(d)^2}[(\tilde{a}(d)U(d) - \tilde{b}(d)V(d))\mathbf{K}_\perp\mathbf{r} + (\tilde{a}(d)V(d) + \tilde{b}(d)U(d))\mathbf{r}], \tag{102}$$

with $\mathbf{v}_{L,2} = -\mathbf{v}_{L,1}$. Hence, the separation vector evolves as

$$\begin{aligned}\frac{d\mathbf{r}}{dt} &= \mathbf{v}_{L,1} - \mathbf{v}_{L,2}\\ &= \frac{\rho_s\kappa^2}{\pi d^2}\frac{1}{\tilde{a}(d)^2 + \tilde{b}(d)^2}[(\tilde{a}(d)U(d) - \tilde{b}(d)V(d))\mathbf{K}_\perp\mathbf{r} + (\tilde{a}(d)V(d) + \tilde{b}(d)U(d))\mathbf{r}].\end{aligned} \tag{103}$$

Writing $\dot{\mathbf{r}} = -\gamma_r^{(\mathrm{HI})}(d)\mathbf{r} + \Omega^{(\mathrm{HI})}(d)\mathbf{K}_\perp\mathbf{r}$, we identify

$$\Omega^{(\mathrm{HI})}(d) = \frac{\rho_s\kappa^2}{\pi d^2}\frac{\tilde{a}(d)U(d) - \tilde{b}(d)V(d)}{\tilde{a}(d)^2 + \tilde{b}(d)^2}, \quad \gamma_r^{(\mathrm{HI})}(d) = -\frac{\rho_s\kappa^2}{\pi d^2}\frac{\tilde{a}(d)V(d) + \tilde{b}(d)U(d)}{\tilde{a}(d)^2 + \tilde{b}(d)^2}. \tag{104}$$

Comparison between hydrodynamic interactions and freely draining cases. The freely draining theory corresponds to $\mu_\perp(d) = 0$ and is recovered from the above by $\tilde{a} \to a$, $\tilde{b} \to b$, $U \to 1$, $V \to 0$. Hydrodynamic interactions preserve the geometric form of the relative motion (a superposition of $\mathbf{r}$ and $\mathbf{K}_\perp\mathbf{r}$), but the two-point coupling $\mu_\perp(d)$ renormalizes both the radial drift and rotation rates into nontrivial functions of separation d. A key qualitative consequence is that, unlike the bare DTDT result where the signs of drift and rotation are fixed by the local coefficients, the HI-resolved rates (104) may change sign as d varies, allowing stalling points and reversals of approach/separation and/or rotation.

The detailed behavior is controlled by the Stokes response in the chosen geometry. In an unbounded domain the transverse interaction mobility is positive and decays with separation, $\mu_\perp(d) > 0$ and $\mu_\perp(d) \to 0$ as $d \to \infty$, so HI acts as a monotone long-range coupling. In periodic domains $\mu_\perp(d)$ remains positive at short separations (where the local flow resembles the unbounded case), but at separations comparable to the box size it can be affected by the global constraints inherent in the periodic Green's function and may change sign. In wall-bounded geometries the interaction mobility is strongly influenced by the boundary conditions and need not have a definite sign [37], so both enhancement and suppression of the freely draining drift/rotation are possible. It is expected that these physics will affect the formation of superfluid vortex structures in the LRT microscales.

B. Two antiparallel straight vortices in an unbounded domain

We consider the same geometry and notation as in the parallel vortices section, but with opposite circulations,

$$\kappa_1 = \kappa, \quad \kappa_2 = -\kappa. \tag{105}$$

In particular, $\mathbf{r} = \mathbf{X}_1 - \mathbf{X}_2$ and $d = \|\mathbf{r}\|$ are defined as before, the undisturbed normal flow is zero ($\bar{\mathbf{v}}_n = \mathbf{0}$), and all operators and vectors are understood on the transverse plane (x, y) with $\mathbf{Q}_\perp = \mathbf{I}_\perp$ and $\mathbf{K}_\perp^2 = -\mathbf{I}_\perp$.

1. Freely draining DTDT

In the absence of hydrodynamic interactions, the normal-fluid velocity entering the drag law is the undisturbed flow, which here is zero, so $\mathbf{v}_n = \mathbf{0}$. The transverse DTDT balance is therefore

$$\mathbf{A}_\perp \, \mathbf{v}_L = \rho_s \kappa \, \mathbf{Q}_\perp \, \mathbf{v}_s = \rho_s \kappa \, \mathbf{v}_s, \quad \mathbf{A}_\perp = a \, \mathbf{I}_\perp + b \, \mathbf{K}_\perp, \tag{106}$$

with

$$a = (\rho_s + \rho_n)\kappa, \quad b = D_\perp. \tag{107}$$

Using $\mathbf{K}_\perp^2 = -\mathbf{I}_\perp$,

$$\mathbf{A}_\perp^{-1} = \frac{1}{a^2 + b^2}(a \, \mathbf{I}_\perp - b \, \mathbf{K}_\perp), \tag{108}$$

and defining (as in the parallel case)

$$\alpha_1 := \rho_s \kappa \, \frac{a}{a^2 + b^2}, \quad \alpha_2 := -\, \rho_s \kappa \, \frac{b}{a^2 + b^2}, \tag{109}$$

we obtain

$$\mathbf{v}_L = \rho_s \kappa \, \mathbf{A}_\perp^{-1} \mathbf{v}_s = \alpha_1 \, \mathbf{v}_s + \alpha_2 \, \mathbf{K}_\perp \, \mathbf{v}_s. \tag{110}$$

For an antiparallel pair ($\kappa_1 = \kappa$, $\kappa_2 = -\kappa$) the induced Biot-Savart velocities at the two lines are equal. Indeed,

$$\mathbf{v}_{s,1} = \frac{\kappa_2}{2\pi d^2} \, \mathbf{K}_\perp \, \mathbf{r} = -\, \frac{\kappa}{2\pi d^2} \, \mathbf{K}_\perp \, \mathbf{r}, \quad \mathbf{v}_{s,2} = \frac{\kappa_1}{2\pi d^2} \, \mathbf{K}_\perp \, (-\mathbf{r}) = -\, \frac{\kappa}{2\pi d^2} \, \mathbf{K}_\perp \, \mathbf{r}, \tag{111}$$

so that

$$\mathbf{v}_{s,1} = \mathbf{v}_{s,2} =: \mathbf{v}_s, \quad \mathbf{v}_s = -\, \frac{\kappa}{2\pi d^2} \, \mathbf{K}_\perp \, \mathbf{r}. \tag{112}$$

Using $\mathbf{K}_\perp^2 = -\mathbf{I}_\perp$ gives

$$\mathbf{K}_\perp \, \mathbf{v}_s = -\, \frac{\kappa}{2\pi d^2} \, \mathbf{K}_\perp^2 \mathbf{r} = \frac{\kappa}{2\pi d^2} \, \mathbf{r}. \tag{113}$$

Inserting in Eq. (110) yields the same line velocity for both vortices,

$$\mathbf{v}_{L,1} = \mathbf{v}_{L,2} = \alpha_1 \, \mathbf{v}_s + \alpha_2 \, \mathbf{K}_\perp \mathbf{v}_s = -\, \frac{\kappa}{2\pi d^2} (\alpha_1 \, \mathbf{K}_\perp \mathbf{r} - \alpha_2 \, \mathbf{r}). \tag{114}$$

Therefore, the separation is constant,

$$\frac{d\mathbf{r}}{dt} = \mathbf{v}_{L,1} - \mathbf{v}_{L,2} = \mathbf{0}, \quad d(t) \equiv d_0, \tag{115}$$

and the pair forms a translating dipole with dipole velocity

$$\mathbf{v}_{\mathrm{dipole}} = \mathbf{v}_{L,1} = \mathbf{v}_{L,2}. \tag{116}$$

Thus, in the freely draining DTDT limit, two antiparallel straight vortices of opposite circulation translate rigidly at fixed separation.

2. DTDT with hydrodynamic interactions

We now include hydrodynamic interactions in the normal component and use the HI-resolved DTDT kinematics (63). For two vortex segments at separation d, the reduced two-point transverse mobility matrix can be parametrized as

$$\mathbf{S}_{\mathrm{full}}(d) = \begin{pmatrix} \sigma_\perp \, \mathbf{I}_\perp & \mu_\perp(d) \, \mathbf{I}_\perp \\ \mu_\perp(d) \, \mathbf{I}_\perp & \sigma_\perp \, \mathbf{I}_\perp \end{pmatrix}, \tag{117}$$

where $\sigma_\perp$ is the transverse self-mobility and $\mu_\perp(d)$ is the (two-point) transverse interaction mobility.

Spectral decomposition of the 4×4 *transverse mobility and symmetric selection.* On the transverse plane the two-point mobility (117) is a 4×4 matrix acting on $\mathbf{F} = (\mathbf{f}_1, \mathbf{f}_2)^\top$ with $\mathbf{f}_i \in \mathbb{R}^2$. It admits the exact projector decomposition

$$\mathbf{S}_{\text{full}}(d) = \lambda_+(d)\,\mathbf{P}_+ + \lambda_-(d)\,\mathbf{P}_-, \quad \lambda_\pm(d) = \sigma_\perp \pm \mu_\perp(d), \quad \mathbf{P}_\pm = \frac{1}{2}\begin{pmatrix} \mathbf{I}_\perp & \pm\mathbf{I}_\perp \\ \pm\mathbf{I}_\perp & \mathbf{I}_\perp \end{pmatrix}. \tag{118}$$

In the present antiparallel configuration, Eq. (112) implies $\mathbf{v}_{s,1} = \mathbf{v}_{s,2}$, and by exchange symmetry the Magnus forcing entering Eq. (63) is symmetric between the two vortices, $\mathbf{f}_{M,2} = \mathbf{f}_{M,1}$. Hence, $\mathbf{F} = (\mathbf{f}, \mathbf{f})^\top$ and

$$\mathbf{P}_-\mathbf{F} = \mathbf{0}, \quad \mathbf{P}_+\mathbf{F} = \mathbf{F}, \tag{119}$$

so that

$$\mathbf{S}_{\text{full}}(d)\,\mathbf{F} = \lambda_+(d)\,\mathbf{F} = (\sigma_\perp + \mu_\perp(d))\,(\mathbf{f}, \mathbf{f})^\top. \tag{120}$$

Therefore, only the symmetric scalar combination $\lambda_+(d) = \sigma_\perp + \mu_\perp(d)$ is sampled in the antiparallel dipole dynamics.

Reduced 2×2 *transverse system.* Restricting $\mathbf{A}$ and $\mathbf{B}$ to the transverse plane gives

$$\mathbf{A}_\perp = a\,\mathbf{I}_\perp + b\,\mathbf{K}_\perp, \quad \mathbf{B}_\perp = \rho_n\kappa\,\mathbf{I}_\perp + b\,\mathbf{K}_\perp. \tag{121}$$

In Eq. (63), the mobility $\mathbf{S}_{\text{full}}$ acts on the force per unit length applied to the normal fluid by the segment. In the Aristotelian DTDT balance this forcing is the Magnus force,

$$\mathbf{f}_M = -\rho_s\kappa\,\mathbf{K}_\perp(\mathbf{v}_L - \mathbf{v}_s), \tag{122}$$

so the HI correction involves $\mathbf{S}_{\text{full}}\mathbf{f}_M$ [as incorporated in Eq. (63)]. By exchange symmetry of the antiparallel pair, the dynamics is confined to the symmetric subspace, so that $\mathbf{v}_{L,2} = \mathbf{v}_{L,1}$ (and likewise for the forcing). Substituting Eq. (117) into Eq. (63) and using the symmetric action (120) yields the exact reduced transverse system for $\mathbf{v}_{L,1}$:

$$(\mathbf{A}_\perp + \rho_s\kappa\,\mu_\perp(d)\,\mathbf{B}_\perp\mathbf{K}_\perp)\mathbf{v}_{L,1} = \rho_s\kappa(\mathbf{I}_\perp + \mu_\perp(d)\,\mathbf{B}_\perp\mathbf{K}_\perp)\mathbf{v}_{s,1}, \quad \mathbf{v}_{L,2} = \mathbf{v}_{L,1}. \tag{123}$$

Using $\mathbf{B}_\perp\mathbf{K}_\perp = -b\,\mathbf{I}_\perp + \rho_n\kappa\,\mathbf{K}_\perp$, define

$$\tilde{a}_+(d) := a - \rho_s\kappa\,b\,\mu_\perp(d), \quad \tilde{b}_+(d) := b + \rho_s\rho_n\kappa^2\,\mu_\perp(d), \tag{124}$$

and

$$U_+(d) := 1 - b\,\mu_\perp(d), \quad V_+(d) := \rho_n\kappa\,\mu_\perp(d). \tag{125}$$

Then Eq. (123) becomes

$$(\tilde{a}_+\,\mathbf{I}_\perp + \tilde{b}_+\,\mathbf{K}_\perp)\mathbf{v}_{L,1} = \rho_s\kappa\,(U_+\,\mathbf{I}_\perp + V_+\,\mathbf{K}_\perp)\mathbf{v}_{s,1}, \tag{126}$$

hence, using $\mathbf{K}_\perp^2 = -\mathbf{I}_\perp$,

$$\mathbf{v}_{L,1} = \frac{\rho_s\kappa}{\tilde{a}_+(d)^2 + \tilde{b}_+(d)^2}[(\tilde{a}_+(d)U_+(d) + \tilde{b}_+(d)V_+(d))\mathbf{I}_\perp + (\tilde{a}_+(d)V_+(d) - \tilde{b}_+(d)U_+(d))\mathbf{K}_\perp]\mathbf{v}_{s,1}, \tag{127}$$

with $\mathbf{v}_{L,2} = \mathbf{v}_{L,1}$.

Dipole translation at fixed separation. For two antiparallel straight vortices one has

$$\mathbf{v}_{s,1} = \mathbf{v}_{s,2} =: \mathbf{v}_s, \quad \mathbf{v}_s = -\frac{\kappa}{2\pi d^2}\mathbf{K}_\perp\,\mathbf{r}, \quad \mathbf{r} = \mathbf{X}_1 - \mathbf{X}_2, \quad d = \|\mathbf{r}\|. \tag{128}$$

Since $\mathbf{v}_{L,2} = \mathbf{v}_{L,1}$, the separation vector is constant,

$$\frac{d\mathbf{r}}{dt} = \mathbf{v}_{L,1} - \mathbf{v}_{L,2} = \mathbf{0}, \quad d(t) \equiv d_0, \tag{129}$$

and the pair forms a translating dipole with velocity $\mathbf{v}_{\text{dipole}} = \mathbf{v}_{L,1}$. Substituting Eq. (128) into Eq. (127) and using $\mathbf{K}_\perp^2 = -\mathbf{I}_\perp$ gives the explicit HI-renormalized dipole velocity

$$\mathbf{v}_{\text{dipole}} = -\frac{\rho_s\kappa^2}{2\pi d^2}\frac{1}{\tilde{a}_+(d)^2 + \tilde{b}_+(d)^2} \times [(\tilde{a}_+(d)U_+(d) + \tilde{b}_+(d)V_+(d))\mathbf{K}_\perp\mathbf{r} - (\tilde{a}_+(d)V_+(d) - \tilde{b}_+(d)U_+(d))\mathbf{r}]. \tag{130}$$

Comparison between hydrodynamic interactions and freely draining cases. The freely draining limit is $\mu_\perp(d) = 0$, so that $\tilde{a}_+ \to a$, $\tilde{b}_+ \to b$, $U_+ \to 1$, $V_+ \to 0$, and Eq. (130) reduces to Eq. (114). In the exact symmetric two-line setting the antiparallel pair remains a rigid dipole, hence

$$\mathbf{v}_{\text{dipole}}(d) = c_K(d)\,\mathbf{K}_\perp\mathbf{r} + c_r(d)\,\mathbf{r}, \quad \mathbf{r} = \mathbf{X}_1 - \mathbf{X}_2, \quad d = \|\mathbf{r}\|, \tag{131}$$

with $c_K(d)$, $c_r(d)$ obtained directly from Eq. (130). Define

$$c_K^{(0)}(d) := c_K(d)\big|_{\mu_\perp=0}, \quad c_r^{(0)}(d) := c_r(d)\big|_{\mu_\perp=0}. \tag{132}$$

A strict reversal of the dipole translation relative to the freely draining prediction is

$$\mathbf{v}_{\text{dipole}}(d)\cdot\mathbf{v}_{\text{dipole}}^{(0)}(d) < 0, \tag{133}$$

which, using $\mathbf{r}\cdot\mathbf{K}_\perp\mathbf{r} = 0$ and $\|\mathbf{K}_\perp\mathbf{r}\|^2 = \|\mathbf{r}\|^2 = d^2$, is equivalent to

$$c_K(d)c_K^{(0)}(d) + c_r(d)c_r^{(0)}(d) < 0. \tag{134}$$

Thus, reversal is controlled solely by the $\mu_\perp(d)$–dependence of $c_K(d)$, $c_r(d)$ via Eq. (130): in geometries where $\mu_\perp(d)$ lacks a definite sign (e.g., periodic or wall-bounded), reversal cannot be excluded *a priori* and must be decided from the computed $\mu_\perp(d)$.

C. Vortex ring in an unbounded domain

We consider a single circular superfluid vortex ring in an otherwise unbounded, and macroscopically quiescent normal fluid. We first recover the familiar shrinking and acceleration in the freely draining (bare DTDT) limit, and then show how the hydrodynamic-interaction (HI) resolved theory modifies these effects in the axisymmetric mode.

1. *Freely draining DTDT*

Let the ring have radius $R(t)$ and lie in the (x, y) plane, centered on the z axis. We parametrize the filament by the azimuthal angle ϕ and use the local orthonormal frame $(\hat{\mathbf{e}}_r, \hat{\boldsymbol{\phi}}, \hat{\mathbf{z}})$, so that the unit tangent is

$$\mathbf{t} = \hat{\boldsymbol{\phi}}. \tag{135}$$

The ring translates along z with speed $U(t) = \dot{Z}(t)$ and its radius evolves with $\dot{R}(t)$. We set the undisturbed normal flow to zero, $\bar{\mathbf{v}}_n = \mathbf{0}$.

In an unbounded superfluid, we can use the standard results for a thin-cored vortex ring in an inviscid, incompressible fluid to evaluate the purely axial, self-induced Biot-Savart velocity of the centerline

$$\mathbf{v}_s = U_s(R)\,\hat{\mathbf{z}}, \quad U_s(R) \simeq \frac{\kappa}{4\pi R}\left[\ln\left(\frac{8R}{\alpha_0}\right) - c_0\right], \tag{136}$$

where α_0 is a defect core radius and $c_0 = O(1)$. For the hollow superfluid vortex cores, we have $c_0 = 1/2$.

In the freely draining DTDT limit the normal fluid entering the local drag law is $\mathbf{v}_n = \bar{\mathbf{v}}_n = \mathbf{0}$, so the overdamped local relation reads

$$\mathbf{A}\,\mathbf{v}_L = \rho_s\kappa\,\mathbf{Q}\,\mathbf{v}_s, \quad \mathbf{A} = a\,\mathbf{I} + b\,\mathbf{K}, \quad \mathbf{K} = [\mathbf{t}\times], \quad \mathbf{Q} = \mathbf{I} - \mathbf{t}\mathbf{t}^\top, \tag{137}$$

with $a = (\rho_s + \rho_n)\kappa$ and $b = D_\perp$.

All physically relevant velocities are in the local plane orthogonal to $\mathbf{t}$, i.e., the $(\hat{\mathbf{e}}_r, \hat{\mathbf{z}})$ plane. Restricting Eq. (137) to this transverse plane, we have $\mathbf{Q}_\perp = \mathbf{I}_\perp$ and $\mathbf{K}_\perp^2 = -\mathbf{I}_\perp$, hence

$$\mathbf{A}_\perp^{-1} = \frac{1}{a^2 + b^2}(a\,\mathbf{I}_\perp - b\,\mathbf{K}_\perp). \tag{138}$$

Defining

$$\alpha_1 := \rho_s\kappa\,\frac{a}{a^2+b^2}, \quad \alpha_2 := -\,\rho_s\kappa\,\frac{b}{a^2+b^2}, \tag{139}$$

we obtain the kinematic law

$$\mathbf{v}_L = \rho_s\kappa\,\mathbf{A}_\perp^{-1}\mathbf{v}_s = \alpha_1\,\mathbf{v}_s + \alpha_2\,\mathbf{K}_\perp\mathbf{v}_s. \tag{140}$$

Using $\mathbf{v}_s = U_s(R)\hat{\mathbf{z}}$ and $\mathbf{K}_\perp\hat{\mathbf{z}} = \mathbf{t}\times\hat{\mathbf{z}} = \hat{\boldsymbol{\phi}}\times\hat{\mathbf{z}} = \hat{\mathbf{e}}_r$, we get

$$\mathbf{v}_L = \alpha_1 U_s(R)\,\hat{\mathbf{z}} + \alpha_2 U_s(R)\,\hat{\mathbf{e}}_r. \tag{141}$$

Therefore,

$$U(t) = \dot{Z}(t) = \alpha_1\,U_s(R), \quad \dot{R}(t) = \alpha_2\,U_s(R). \tag{142}$$

Since $b = D_\perp > 0$, we have $\alpha_2 < 0$, so $\dot{R} < 0$ and the ring shrinks. Moreover $U_s(R)$ increases as R decreases, so the ring accelerates as it shrinks. Thus, the freely draining DTDT reproduces the standard shrinking/acceleration behavior in closed form.

2. DTDT with hydrodynamic interactions

We now include the LRT hydrodynamic interactions through the HI-resolved DTDT dynamics. We use the derived vortex dynamics equations in terms of the off-diagonal mobility (with $\bar{\mathbf{v}}_n = \mathbf{0}$):

$$(\mathbf{A}_\perp + \rho_s\kappa\,\mathbf{B}_\perp\,\mathbf{S}_{\text{off}}\,\mathbf{K}_\perp)\mathbf{v}_L = \rho_s\kappa(\mathbf{I}_\perp + \mathbf{B}_\perp\,\mathbf{S}_{\text{off}}\,\mathbf{K}_\perp)\mathbf{v}_s, \quad \mathbf{B}_\perp = \rho_n\kappa\,\mathbf{I}_\perp + b\,\mathbf{K}_\perp. \tag{143}$$

In the axisymmetric ring evolution (ring remains circular; only $R(t)$ and $Z(t)$ evolve), the forcing applied to the normal fluid is uniform along the ring in the local transverse basis. Rotational symmetry then implies that the total off-diagonal response is also uniform along the ring. However, the ring geometry distinguishes $\hat{\mathbf{e}}_r$ (curvature normal) from $\hat{\mathbf{z}}$ (axis), so the axisymmetric off-diagonal mobility is, in general, a diagonal 2×2 map on the transverse plane:

$$\boxed{\mathbf{S}_{\text{off}}(R)\big|_{m=0} \equiv \boldsymbol{\mu}_0(R) := \mu_r(R)\,\hat{\mathbf{e}}_r\hat{\mathbf{e}}_r^\top + \mu_z(R)\,\hat{\mathbf{z}}\hat{\mathbf{z}}^\top.} \tag{144}$$

Substituting $\mathbf{S}_{\text{off}} \to \boldsymbol{\mu}_0(R)$ into Eq. (143) gives a closed 2×2 transverse linear system for $\mathbf{v}_L$.

Closed expressions for translation and shrinking. Write $\mathbf{v}_L = v_r\,\hat{\mathbf{e}}_r + v_z\,\hat{\mathbf{z}}$ and $\mathbf{v}_s = U_s(R)\hat{\mathbf{z}}$. In the basis $(\hat{\mathbf{e}}_r, \hat{\mathbf{z}})$ one has

$$\mathbf{K}_\perp = \begin{pmatrix} 0 & 1 \\ -1 & 0 \end{pmatrix}, \quad \boldsymbol{\mu}_0(R) = \begin{pmatrix} \mu_r(R) & 0 \\ 0 & \mu_z(R) \end{pmatrix}.$$

Solving Eq. (143) yields

$$\boxed{\dot{R} = v_r = \frac{\rho_s\kappa\,U_s(R)}{\Delta(R)}[(\rho_n\kappa)\,\mu_r(R)\,(a - \rho_s\kappa\,b\,\mu_r(R)) - (b + \rho_s\rho_n\kappa^2\,\mu_r(R))(1 - b\,\mu_r(R))],} \tag{145}$$

$$\boxed{\begin{aligned} U(R) &= \dot{Z} = v_z \\ &= \frac{\rho_s\kappa\, U_s(R)}{\Delta(R)}[(a - \rho_s\kappa\, b\, \mu_z(R))(1 - b\, \mu_r(R)) + (\rho_n\kappa)\, \mu_r(R)\, (b + \rho_s\rho_n\kappa^2\, \mu_z(R))], \qquad (146) \end{aligned}}$$

with the denominator

$$\boxed{\Delta(R) := (a - \rho_s\kappa\, b\, \mu_z(R))(a - \rho_s\kappa\, b\, \mu_r(R)) + (b + \rho_s\rho_n\kappa^2\, \mu_r(R))(b + \rho_s\rho_n\kappa^2\, \mu_z(R)).} \quad (147)$$

Setting $\mu_r = \mu_z = 0$ gives $\Delta = a^2 + b^2$ and Eqs. (145) and (146) reduce exactly to the bare relations (142). Hence, hydrodynamic interactions preserve the geometric structure of the axisymmetric ring dynamics but renormalize translation and shrinking through *two* distinct couplings, $\mu_r(R)$ and $\mu_z(R)$, allowing HI to affect $\dot{R}$ and U in different ways.

In the bare (freely draining) theory one has $\dot{R} = \alpha_2 U_s(R)$ with $\alpha_2 < 0$ for $D_\perp > 0$, hence the ring always shrinks. In the HI-resolved theory, $\dot{R}$ is given by Eq. (145) in the form $\dot{R} = N_R(R)/\Delta(R)$, where $\Delta(R)$ is the determinant of the 2×2 matrix multiplying $\mathbf{v}_L$ on the left-hand side of the axisymmetric HI closure in the $(\hat{\mathbf{e}}_r, \hat{\mathbf{z}})$ basis. Stalling radii $R = R_*$ satisfy $N_R(R_*) = 0$ provided $\Delta(R_*) \neq 0$ (nonsingular transverse closure). A reversal of shrinking/expansion requires a sign change of the ratio $N_R(R)/\Delta(R)$: this may occur via a sign change of N_R at fixed sign of Δ, or via a sign change of Δ at fixed sign of N_R. The case $\Delta(R) = 0$ corresponds to loss of invertibility of the overdamped HI closure and requires separate treatment. Thus, unlike bare DTDT, the HI-resolved theory permits stalling and reversals in principle, with the actual behavior set by the computed functions $\mu_r(R)$ and $\mu_z(R)$ in the chosen geometry and regularization.

V. FORMULATION OF FINITE-TEMPERATURE SUPERFLUID TURBULENCE HYDRODYNAMICS WITH HYDRODYNAMIC INTERACTIONS

Up to this point we have formulated superfluid vortex dynamics with hydrodynamic interactions in the LRT regime, and we have illustrated their impact on canonical vortex configurations, highlighting departures from the freely draining limit that can affect how discrete topological defects interact and form structures at mesoscopic (LRT) scales. In effect, we have extended the microhydrodynamic/LRT interaction framework, familiar from classical statistical systems such as polymeric and granular fluids, to the finite-temperature quantum setting, while accounting for the key difference that superfluid vortices are topological defects rather than material particles.

Many major superfluid applications, from cryogenic flows to neutron-star interiors, involve strongly fluctuating turbulent fields at hydrodynamic scales that are separated by many orders of magnitude from the LRT microflows resolved by the present defect-normal-fluid coupling. We therefore face the central multiscale challenge: how can the small-scale LRT hydrodynamic interactions be incorporated into the coupled vortex and normal-fluid dynamics while still using computationally feasible discretizations, and while retaining asymptotic exactness in the scale-separated limit?

In what follows we present a continuum formulation of finite-temperature superfluid turbulence that meets these requirements. The key step is to project the LRT microflow effects onto the hydrodynamic description of the normal fluid, thereby obtaining an effective turbulent-scale system that remains consistent with the underlying Stokes/LRT response. We then formulate the resulting coupled equations in a form amenable to computation, and outline corresponding numerical and algorithmic procedures for their solution.

Beyond formal consistency, a central goal of this work is computational viability for physically realistic turbulent flows. The formulation developed here closes the coupled defect-normal-fluid dynamics across the entire continuum range above the relaxation scales by coupling an overdamped (Stokes/LRT) microflow response to a hydrodynamic (Navier-Stokes) description at large scales.

This provides a first-principles pathway for incorporating hydrodynamic interactions and mutual-friction microphysics into turbulence calculations without resolving the prohibitive LRT length scales on the computational grid, while remaining asymptotically exact in the scale-separated limit. In this sense the theory links the discrete topological-defect dynamics to the continuum turbulent regime through an explicit, computable projection, and yields new predictive content at hydrodynamic scales via an effective stress of LRT origin. The framework is also boundary-condition agnostic: periodic and wall-bounded geometries enter only through the Stokes/LRT mobility returned by the solver. The required self-term $\sigma_\perp$ is obtained consistently from the same solver via a single-segment probe (tabulated near walls if needed).

A. Key time and length scales

A central difficulty in formulating an asymptotically exact continuum description of finite-temperature superfluid turbulence is the coexistence of multiple, physically distinct small length and timescales. Because of the enormous computational cost, it is not feasible to resolve motions on all relevant space-timescales. In this section we outline an effective-dynamics strategy that enables the calculation of the turbulent scales of interest while retaining the full LRT physics.

At hydrodynamic scales, the normal component supports inertial turbulence, while the superfluid vorticity is carried by a network of quantized vortex filaments whose total extent is comparable to the system size. The two components are coupled by mutual-friction and Iordanskii forces concentrated on the filaments. A brute-force continuum simulation of the coupled system would therefore have to resolve, in addition to the Kolmogorov scale of normal-fluid turbulence, the small-amplitude LRT microflows driven by these line-supported forces. Since the LRT motions are driven by line-supported (delta-function) forcing, such a direct resolution is not feasible in practice.

Our strategy is therefore to use a hydrodynamic grid that resolves the turbulent normal-fluid motions down to a cutoff that resolves both viscous and mutual-friction damping processes, and to replace the bare coupled equations by an *effective* hydrodynamic-scales system obtained by filtering at that cutoff. The filtered equations retain the resolved turbulence dynamics but acquire an additional stress that represents the impact of the unresolved LRT microflows. The same LRT physics also enters the line-supported coupling forces, because in the present theory the normal-fluid velocity sampled in the defect drag law includes full HI effects. The unresolved LRT response below the filter scale is computed separately by an overdamped Stokes/LRT solver (e.g., P3M), consistent with the mobility framework used above for defect hydrodynamic interactions. This two-level description is asymptotically exact in the scale-separated limit in which the LRT response is fast compared with the smallest resolved turbulent timescales, so that the microflow adjusts quasi-instantaneously to the slowly evolving hydrodynamic fields.

Importantly, this time-scale separation is not an additional modeling assumption: it is an asymptotic consequence of the overdamped (Aristotelian) vortex dynamics adopted throughout, i.e., of the negligible effective vortex inertia. In this regime the LRT normal-fluid response to line forcing is rapidly relaxing, so the HI microflow is slaved to the instantaneous hydrodynamic fields even when the corresponding *length*-scale separation is not extreme.

Finally, the normal-fluid and filament discretizations need not coincide. The vortex dynamics must resolve Kelvin waves along the linear defects, whereas the hydrodynamic grid resolves the normal-fluid turbulence down to its damping scale; the present formulation couples these two resolutions consistently through the combination of filtered equations at hydrodynamic scales and the Stokes equations at LRT scales.

1. Vortex dynamical scales

Vortex discretization scale. As already mentioned in Sec. II A, mutual friction damps Kelvin-wave excitations along superfluid vortex filaments. Samuels and Kivotides showed that this introduces a characteristic damping (cutoff) length scale $\ell_{\rm sd}$, below which vortex distortions are strongly attenuated and do not survive dynamically. Consequently, the vortex dynamics need only be resolved down to this scale.

Accordingly, the arclength discretization along superfluid vortices, $\delta\ell_{\mathrm{v}}$, must satisfy

$$\delta\ell_{\mathrm{v}} \lesssim \frac{\lambda_c}{2}, \quad \lambda_c \sim \ell_{\mathrm{sd}}, \tag{148}$$

so that Kelvin-wave content below the physical cutoff wavelength λ_c is neither dynamically present nor numerically represented.

Reconnection threshold scale. In vortex-filament dynamics reconnections are not resolved at the level of core physics, but are implemented topologically as cut–swap operations. The key modeling input is therefore a reconnection threshold scale ℓ_{rec}, which specifies when two approaching filaments are deemed to have entered a one-way route to reconnection. Indeed, as indicated by de Waele and Aarts [38], when two vortices approach each other beyond a critical separation a pyramidal-like contour instability forms that leads to reconnection. In a vortex–filament description this motivates a *mesoscopic* trigger that identifies when a close encounter has entered the universal close-approach (pyramidal-structure) regime, formulated directly in terms of interactions.

Before specifying the particular trigger used here, it is useful to note that vortex-filament calculations employ a family of operational reconnection prescriptions. These range from simple geometrical proximity rules to more dynamical criteria based on the predicted crossing of line elements during the next time step. Representative vortex-filament implementations include Schwarz [39], Samuels [40], Tsubota, Araki and Nemirovskii [41], Adachi, Fujiyama and Tsubota [42], and Kondaurova and Nemirovskii [43].

The present work uses the physical route to reconnection identified by de Waele and Aarts [38] as the basis for a mesoscopic trigger criterion. The reason for introducing this criterion is that geometrical proximity alone does not necessarily imply the physical plausibility of reconnection.

Line tension (local restoring interaction). The kinetic energy of the swirling superflow around a thin vortex core implies an effective line tension (energy per unit length)

$$T \simeq \frac{\rho_s\kappa^2}{4\pi} \ln\left(\frac{\ell_o}{\alpha_0}\right), \tag{149}$$

with outer cutoff ℓ_o set by the local environment. We take $\ell_o = \min(R_0, \delta_{iv}^{\mathrm{local}})$, where $R_0 = 1/|\partial^2\mathbf{X}/\partial\xi^2|$ is the local radius of curvature (ξ the arclength parameter), and $\delta_{iv}^{\mathrm{local}}$ is the local intervortex spacing in inhomogeneous tangles. We estimate

$$\delta_{iv}^{\mathrm{local}} = \sqrt{\mathcal{V}_{\mathrm{loc}}/L_{\mathrm{loc}}} = \lambda_{\mathrm{loc}}^{-1/2}, \tag{150}$$

where $\mathcal{V}_{\mathrm{loc}}$ is a local coarse-graining volume surrounding the candidate closest-approach region, L_{loc} is the total vortex length contained in $\mathcal{V}_{\mathrm{loc}}$, and $\lambda_{\mathrm{loc}} = L_{\mathrm{loc}}/\mathcal{V}_{\mathrm{loc}}$ is the corresponding local vortex-line density.

We choose $\ell_o = \min(R_0, \delta_{iv}^{\mathrm{local}})$ because two effects can terminate the single-filament, locally straight description used in the tension logarithm: (i) bending on the curvature scale R_0, and (ii) loss of isolation due to neighboring vortices at spacing $\delta_{iv}^{\mathrm{local}}$. The relevant outer cutoff is the smaller of these, since beyond $\delta_{iv}^{\mathrm{local}}$ the filament is not isolated, while beyond R_0 the locally straight approximation fails. The corresponding restoring force per unit length is

$$|f_{\mathrm{tens}}| \sim \frac{T}{R_0}. \tag{151}$$

Nonlocal interaction of a close pair. Two nonneighboring segments at distance δ interact hydrodynamically; the interaction force per unit length scales as

$$|f_{\mathrm{nl}}| \sim \frac{\rho_s|\kappa_1\kappa_2|}{2\pi}\,\frac{1}{\delta}, \tag{152}$$

up to an $O(1)$ geometric factor. The nonlocal interaction may be either attractive (locally antiparallel) or repulsive (locally parallel); (152) provides an estimate of its magnitude in both cases.

Reconnection trigger distance. We define entry into the de Waele–Aarts reconnection route by dominance of nonlocal interaction over vortex tension, $|f_{\mathrm{nl}}| \gtrsim |f_{\mathrm{tens}}|$. Since a reconnection may be initiated by the instability of either filament, we evaluate $|f_{\mathrm{tens}}|$ for both filaments at the candidate closest points and use the smaller value (equivalently, the smaller of the two local curvature radii). Using (149)–(152) we obtain the trigger distance

$$\delta_{\mathrm{rec}} \sim \frac{2R_0}{\ln(\ell_o/\alpha_0)}. \tag{153}$$

Thus, the trigger scale is a *fraction* of the local geometric scale R_0, reduced by the logarithm $\ln(\ell_o/\alpha_0)$, rather than the core scale at which the actual topological change occurs. For $\ell_o/\alpha_0 \in [10^4, 10^6]$ we have $2/\ln(\ell_o/\alpha_0) \approx 0.15 \pm 0.05$, so this ratio may be treated as a slowly varying $O(0.1)$ factor.

Finally, since reconnections transform kinetic energy into compressible excitations that are not represented in our incompressible filament dynamics, we perform only those reconnections that decrease the total vortex length.

2. Normal-fluid scales

Smallest normal-fluid scales (resolution criterion). The aim here is purely to estimate the smallest dynamically active normal-fluid length scales to guide numerical resolution. Full nondimensionalization of the coupled system is elaborated in Appendix B. We therefore use the Kolmogorov time-scale criterion [44]: in an inertial cascade with energy flux ε, eddies of size ℓ have a turnover time

$$\tau_\ell \sim \frac{\ell}{u_\ell} \sim \varepsilon^{-1/3}\ell^{2/3}, \tag{154}$$

where $u_\ell \sim (\varepsilon\ell)^{1/3}$ in the inertial range. The smallest dynamically active scales are identified by matching this inertial time to the shortest noninertial timescales introduced by dissipative or exchange mechanisms.

Viscosity provides the classical diffusion time $\tau_\nu(\ell) \sim \ell^2/\nu$, which yields the Kolmogorov scale

$$\eta_\nu \sim \left(\frac{\nu^3}{\varepsilon}\right)^{1/4}. \tag{155}$$

In the present two-fluid setting the defect-induced terms introduce additional characteristic rates. In the normal-fluid equation, mutual-friction action enters with a kinematic coefficient ν_c (with $\nu_c/\nu \sim O(1)$ as already discussed), so that its small-scale action can be characterized by the timescale

$$\tau_{mf}(\ell) \sim \frac{\ell^2}{\nu_c}. \tag{156}$$

Equating τ_ℓ and $\tau_{mf}(\ell)$ yields the mutual-friction crossover scale

$$\ell_{mf} \sim \left(\frac{\nu_c^3}{\varepsilon}\right)^{1/4}, \tag{157}$$

which is therefore comparable to η_ν when $\nu_c/\nu \sim O(1)$.

The Iordanskii contribution is conservative in the combined two-fluid system but introduces an exchange/deflection rate characterized by the kinematic coefficient κ (with $\kappa/\nu \sim O(1)$ for ^{4}He in the relevant temperature range). Dimensional consistency then implies the associated characteristic timescale

$$\tau_I(\ell) \sim \frac{\ell^2}{\kappa}, \tag{158}$$

and time-scale matching $\tau_\ell \sim \tau_I(\ell)$ gives the corresponding crossover length

$$\ell_I \sim \left(\frac{\kappa^3}{\varepsilon}\right)^{1/4}. \tag{159}$$

In other words, energy injection by defect-induced forces at scales larger than the cascade terminus merely feeds the inertial range and is passed down the cascade; it does not change the smallest dynamically active scale. Only when the characteristic mutual-friction or Iordanskii time becomes comparable to the smallest inertial turnover time does their associated crossover scale coincide with the cascade cut-off.

We therefore estimate the smallest turbulent normal-fluid length as

$$\ell_{\min} \sim \max(\eta_\nu,\ \ell_{mf},\ \ell_I). \tag{160}$$

Below this scale there are no dynamically active turbulent motions in the normal fluid, but only the LRT (creeping/Stokes) microflows whose effect on the vortex dynamics was the focus of the previous sections. Using these scale estimates, we next formulate a resolved normal-fluid turbulence model that is informed by the subgrid LRT microflow patterns without explicitly resolving them. Notably, for superfluid ^{4}He the additional cutoff scales ℓ_{mf} and ℓ_I are of the same order as the classical Kolmogorov scale η_ν. This justifies the use by Samuels and Kivotides of η_ν as an effective cutoff for normal-fluid turbulence in their specification of the superfluid vortex-dynamics cutoff ℓ_{sd}.

B. Filtering the formal system

The real issue with computing superfluid turbulent flows is the enormous resolution that would be required to simultaneously resolve the turbulent normal-fluid motions and the LRT microflows. The vortex-dynamics part does not present a comparable *resolution* bottleneck because, in turbulent flows, the computational mesh along the topological defects is not set by the detailed LRT microflow patterns, but by the smallest Kelvin-wave content that remains dynamically active under the action of the resolved normal-fluid motions, as argued by Samuels and Kivotides.

The theory developed in earlier sections can efficiently predict superfluid vortex motions given (i) a P3M/Stokes solver for the LRT flows and hydrodynamic interactions, and (ii) the *undisturbed* normal-fluid velocity field. Here "undisturbed" is used in the standard Stokesian sense: it is the large-scale (resolved) normal-fluid field sampled on the filament with the LRT disturbance induced by the vortex configuration removed; at the same time it is the field *informed* by the action of mutual-friction and Iordanskii forces through the large-scale normal-fluid dynamics.

Therefore, to resolve all dynamically relevant scales in both superfluid and normal-fluid degrees of freedom, what is needed is an algorithm that advances, via Navier-Stokes dynamics, only the turbulent normal-fluid scales, while accounting for the effect of the unresolved LRT motions. To achieve this, we follow a procedure proposed by Kivotides [45] in the context of complex fluids: we *filter* the Navier-Stokes equation at the cutoff scale specified above, and we indicate how the resulting filtered system incorporates the influence of the *unresolved* LRT motions. This formulation is accurate provided the LRT response is rapid compared with the evolution time of the filtered hydrodynamic motions. This condition follows from the physical separation between LRT and hydrodynamic scales: LRT microflows are overdamped (Stokesian) and relax rapidly compared with the turnover time of the smallest resolved turbulent eddies, consistent with the Aristotelian limit of the vortex dynamics used in subsequent sections. Thus, the treatment that follows is a controlled and accurate approximation while retaining computational feasibility.

The filtering operation. Let G_{Δ_n} denote the normal-fluid filter at grid spacing Δ_n, with $\Delta_n \leqslant \ell_{\min}$ so that the grid resolves all turbulent eddies. Following the analysis of Ref. [45], we assume that G_{Δ_n} is an idempotent *projector* onto the resolved continuum scales: for any field ϕ,

$$\bar{\phi}(\mathbf{x}, t) = \int_\Omega \phi(\mathbf{y}, t)\, G_{\Delta_n}(\mathbf{x} - \mathbf{y})\, d^3y, \quad \bar{\bar{\phi}} = \bar{\phi}, \quad \bar{1} = 1, \tag{161}$$

where Ω is the computational domain. Equivalently, in Fourier space one may view G_{Δ_n} as a sharp spectral projector, $\widehat{G}(\mathbf{k}) = 1$ for $|\mathbf{k}| \leqslant k_c$ and 0 otherwise, with $\Delta_n \sim k_c^{-1}$. More generally, suitable filters have even kernels, $G_{\Delta_n}(\mathbf{x}) = G_{\Delta_n}(-\mathbf{x})$, satisfy $\int_{\mathbb{R}^3} G_{\Delta_n}(\mathbf{x})\, d^3x = 1$, and are localized on $|\mathbf{x}| \lesssim \Delta_n$ [45] (e.g., box, Gaussian, and sharp spectral filters). In what follows we assume the projector properties (161) and that filtering commutes with differentiation.

We use the standard decomposition

$$\mathbf{v}_n(\mathbf{x}, t) = \bar{\mathbf{v}}_n(\mathbf{x}, t) + \mathbf{v}_n'(\mathbf{x}, t), \quad p(\mathbf{x}, t) = \bar{p}(\mathbf{x}, t) + p'(\mathbf{x}, t), \tag{162}$$

and similarly for any other normal-fluid quantity.

The vortex forcing is supported on the filament set $\mathcal{L}(t)$ parametrized by $\mathbf{X}(\xi, t)$ and may be written in distributional form as

$$\mathbf{f}(\mathbf{x}, t) = \int_{\mathcal{L}(t)} \mathbf{f}^{\text{line}}(\xi, t)\, \delta^{(3)}(\mathbf{x} - \mathbf{X}(\xi, t))\, d\xi, \tag{163}$$

where $\mathbf{f}^{\text{line}}$ is the force per unit vortex length exerted by the filaments on the normal fluid (mutual friction plus Iordanskii). Although Eq. (163) is written using $\delta^{(3)}$, the forcing is line-supported and thus codimension–2: it is singular only in the two directions transverse to the local tangent.

Applying the projector filter G_{Δ_n} to Eq. (163) replaces $\delta^{(3)}$ by G_{Δ_n} and yields the regularized body-force density on the normal-fluid grid,

$$\bar{\mathbf{f}}(\mathbf{x}, t) = \int_{\mathcal{L}(t)} \mathbf{f}^{\text{line}}(\xi, t)\, G_{\Delta_n}(\mathbf{x} - \mathbf{X}(\xi, t))\, d\xi. \tag{164}$$

1. Filtered equations skeleton for the coupled superfluid problem

The method advances simultaneously: (i) the resolved normal-fluid velocity $\bar{\mathbf{v}}_n(\mathbf{x}, t)$, (ii) the vortex configuration $\mathcal{L}(t)$, and (iii) the deterministic Stokes/LRT microflow induced by the line forcing, which provides HI and an exact evaluation of the subfilter stress.

Filtered normal-fluid equations. The filtered incompressibility constraint is, in component form,

$$\frac{\partial \bar{v}_{n,i}}{\partial x_i} = 0. \tag{165}$$

Filtering the incompressible normal-fluid momentum equation written in conservative (flux) form gives

$$\begin{aligned} &\rho_n \frac{\partial \bar{v}_{n,i}}{\partial t} + \rho_n \frac{\partial (\bar{v}_{n,i}\bar{v}_{n,j})}{\partial x_j} + \frac{\partial \bar{p}}{\partial x_i} + \rho_n \frac{\partial \overline{v_{n,i}' v_{n,j}'}}{\partial x_j} - \mu\, \frac{\partial^2 \bar{v}_{n,i}}{\partial x_j \partial x_j} \\ &\quad + \int_{\mathcal{L}(t)} f_i^{\text{line}}(\xi, t)\, G_{\Delta_n}(\mathbf{x} - \mathbf{X}(\xi, t))\, d\xi = 0, \end{aligned} \tag{166}$$

with $\mu := \rho_n \nu$. The only term not yet specified is the residual stress $\rho_n\, \overline{v_{n,i}' v_{n,j}'}$, which we evaluate below from the LRT microflow.

Vortex dynamics in the Aristotelian limit. The filament centerlines satisfy $\partial_t \mathbf{X} = \mathbf{v}_L$, with $\mathbf{v}_L$ determined by Eq. (63) derived in earlier sections,

$$\mathbf{v}_L = (\mathbf{A}_{\text{eff}} \;+\; \rho_s \kappa\, \mathbf{B}\, \mathbf{S}_{\text{full}} \mathbf{K})^{-1} \mathbf{R}_{\text{eff}},$$

with $\mathbf{A}_{\text{eff}}$ and $\mathbf{R}_{\text{eff}}$ given by Eqs. (59) and (62), and $\sigma_\perp$ the transverse self-term (a single scalar) associated with the chosen periodic box, P3M kernel and core model. The key point is that the “undisturbed” normal-fluid velocity $\bar{\mathbf{v}}_n$ entering this equation is the filtered field of Eq. (166).

Stokes/LRT microflow for hydrodynamic interactions. The subfilter normal-fluid response induced by the line forcing is computed from the instantaneous creeping-flow problem (e.g., via a P3M method). The Stokes/LRT equations are

$$\frac{\partial v^S_{n,i}}{\partial x_i} = 0, \tag{167}$$

$$\frac{\partial p^S}{\partial x_i} - \mu \frac{\partial^2 v^S_{n,i}}{\partial x_j \partial x_j} + \int_{\mathcal{L}(t)} f_i^{\mathrm{line}}(\xi, t)\, \delta^{(3)}(\mathbf{x} - \mathbf{X}(\xi, t))\, d\xi = 0. \tag{168}$$

The details of the method are described in Ref. [45] and are not intrinsically related to superfluid physics. They apply to all LRT flows. The P3M method splits the Stokes/LRT field into a rapidly varying local part and a slowly varying global part,

$$\mathbf{v}^S_n = \mathbf{v}^S_{n,l} + \mathbf{v}^S_{n,g}. \tag{169}$$

We follow the analysis of Ref. [45] in choosing the splitting parameters so that $\mathbf{v}^S_{n,g}$ varies on scales $\gtrsim \Delta_n$, i.e., on the same scales as $\bar{\mathbf{v}}_n$. The local part $\mathbf{v}^S_{n,l}$ carries the short-range response to the line-supported forcing and decays rapidly above the Δ_n scales. Since the filtered Navier-Stokes equation resolves all scales above Δ_n, and $\mathbf{v}^S_{n,g}$ varies on scales $\gtrsim \Delta_n$, the subgrid residual stress $\tau^R_{ij} = -\rho_n\, \overline{v'_{n,i} v'_{n,j}}$ can be evaluated solely in terms of $\mathbf{v}^S_{n,l}$, the LRT modes that exist below the filtering scale. Details of the exact residual-stress evaluation are given in Appendix A.

2. *Computational algorithm*

Solutions of the coupled system can be obtained by the following algorithm:

(1) *Initial data.* At $t = 0$ prescribe the initial vortex tangle configuration $\mathcal{L}(0)$, an initial filament velocity $\mathbf{v}_L(\xi, 0)$ (e.g., $\mathbf{v}_L(\xi, 0) = 0$), and the resolved incompressible normal-fluid field $\bar{\mathbf{v}}_n(\mathbf{x}, 0)$. Using $\mathcal{L}(0)$, evaluate the superfluid velocity sampled on the filaments, $\mathbf{v}_s(\mathbf{X}(\xi, 0), 0)$.

(2) *Filament forcing (Magnus/line force).* Using the current filament geometry and velocities, evaluate the Magnus force on the filaments and, by action-reaction in the Aristotelian (force-balance) limit, the corresponding line force per unit length exerted by the filaments on the normal fluid, $\mathbf{f}^{\mathrm{line}}(\xi, t)$.

(3) *Stokes/LRT microflow and mobility data.* Solve the forced Stokes/LRT problem with line forcing $\mathbf{f}^{\mathrm{line}}$ (e.g., via a P3M method) to obtain the microflow field $\mathbf{v}^S_n$ and its split $\mathbf{v}^S_n = \mathbf{v}^S_{n,l} + \mathbf{v}^S_{n,g}$, together with the mobility quantities $\mathbf{S}_{\mathrm{full}}$ and $\sigma_\perp$.

(4) *Filament velocity.* Insert the above quantities into the vortex-dynamics law (63) and compute the filament velocity $\mathbf{v}_L(\xi, t)$.

(5) *Advance the tangle and refresh forcing.* Integrate $\partial_t \mathbf{X} = \mathbf{v}_L$ over one time step to update the filament configuration $\mathcal{L}(t) \mapsto \mathcal{L}(t + \Delta t)$, and recompute $\mathbf{v}_s$ on the updated filaments. Using the updated geometry and velocities, re-evaluate the Magnus force and hence the updated line forcing $\mathbf{f}^{\mathrm{line}}(\xi, t + \Delta t)$.

(6) *Subgrid stress.* Using the local Stokes field $\mathbf{v}^S_{n,l}$, evaluate the residual-stress term in the filtered Navier-Stokes equation.

(7) *Resolved normal-fluid update.* Insert the updated forcing $\mathbf{f}^{\mathrm{line}}(\xi, t + \Delta t)$ into the filtered Navier-Stokes equation, and solve the filtered system to obtain the updated resolved normal-fluid fields $(\bar{\mathbf{v}}_n, \bar{p})$ at $t + \Delta t$.

(8) *Time marching.* Set $t \leftarrow t + \Delta t$ and return to step 2 until the desired final time is reached.

This algorithm is applicable to arbitrary boundary conditions, normal-fluid flow types, and vortex line densities, subject only to computational complexity limitations.

VI. CONCLUDING REMARKS

This work is based on a separation of superfluid physics into two realms: (i) the microscopic quantum-statistical (many-body) description from which effective two-fluid and defect dynamics emerge, and (ii) the continuum (field) description applicable above the normal-fluid relaxation scales, where both the thermal excitations and the superfluid are represented by continuous fields. Within the continuum realm—which comprises two subregimes, the mesoscopic Linear-Response and the macroscopic hydrodynamic ranges of scales—the superfluid contains topological defects (vortex filaments) whose dynamics are coupled to the normal-fluid field through dissipative (mutual-friction) and reactive (Iordanskii) mechanisms. We have developed a formulation that captures the coupled continuum dynamics of a normal fluid of thermal excitations interacting with such discrete defects, while retaining for the first time in superfluids an explicit LRT microhydrodynamic response—used both to drive filament motion via the filament-sampled normal-fluid velocity $\mathbf{v}_n(\mathbf{X}, t)$ and to close the filtered normal-fluid equations through the residual stress.

To achieve this, we merged the hydrodynamic and LRT regimes into a single consistent continuum description. On the defect side, we incorporated LRT HI between vortices into the vortex dynamics, and showed that this inclusion leads to qualitative changes in elementary configurations, including parallel and anti-parallel line pairs and the motion of a single ring in an otherwise quiescent normal fluid. On the normal-fluid side, we coarse-grain the Navier-Stokes dynamics at a cutoff Δ_n while resolving all turbulent motions above Δ_n. The influence of LRT modes on the resolved turbulence enters through two channels: (i) a subfilter (residual) stress generated by the local Stokes/LRT microflow below Δ_n, and (ii) HI-informed defect reaction forces, since the coupling laws sample the full filament-scale normal-fluid velocity rather than a freely draining approximation. We further show how the subfilter stress can be evaluated in an asymptotically exact manner at fixed cutoff Δ_n.

To make the application of this theory concrete, we present a detailed algorithmic procedure integrating the coupled normal-fluid and vortex-dynamics solvers with a Stokesian (LRT) P3M scheme. In the Appendixes, we provide (i) a methodology for computing the subfilter stress and (ii) a scaling analysis of the coupled vortex-dynamics/filtered-normal-fluid system. We conclude with remarks that place the formulation in a broader context.

(1) Analogy with classical turbulence closures. In Navier-Stokes turbulence one seeks an effective description of unresolved fluctuations (e.g., Reynolds stresses), yet systematic derivations from statistical mechanics are obstructed by strong nonlinearity. In practice, major progress has relied on numerical resolution of the governing equations, which then informed useful closure models.

Superfluids face an analogous challenge. Large-scale descriptions in the spirit of HVBK require constitutive input describing how vortex structures organize and how they couple to normal-fluid eddies under general flow and boundary conditions. Phenomenological models may succeed in special settings, but broadly predictive closure laws are difficult to derive systematically.

A fully coupled numerical route encounters an additional obstacle: defect forcing enters the hydrodynamic equations as distributional sources, while the defect velocities that determine that forcing are controlled by physics at smaller (LRT) scales. The aim of the present work has been to bridge the hydrodynamic and LRT regimes in a controlled and accurate manner, providing a principled route to continuum modeling without discarding the microhydrodynamics that controls defect motion.

(2) Computational complexity of superfluid turbulence. Superfluids are computationally more demanding than standard complex fluids of statistical physics. In granular or polymeric flows the number of degrees of freedom is fixed, whereas in superfluids the number of vortex degrees of freedom is not conserved: it can grow dramatically through line stretching and the associated increase of total vortex length. Addressing this reliably calls for advanced massively parallel algorithms, for example GPU-based implementations of the present formalism.

(3) Multidisciplinary character and diverse applications. The present formulation extends low–Reynolds-number hydrodynamics, familiar from granular and polymeric complex fluids, to the dynamics of symmetry-breaking-induced topological defects in quantum fluids. In particular, the inclusion of the nondissipative Iordanskii coupling introduces a reactive component to defect-normal-fluid interactions, leading to an effective mobility description with distinct dissipative and reactive contributions in the vortex-dynamics equations. This viewpoint creates a natural interface

between the superfluid and complex-fluids communities, especially in the development of fast Stokes/LRT solvers and integrators under realistic boundary conditions, with applications ranging from laboratory and cryogenic flows to astrophysical superfluids (e.g., neutron-star interiors).

(4) Generality of the formulation. The formalism is deliberately general and admits several natural extensions. It can be adapted to a wide range of boundary conditions, including unbounded domains, periodic geometries, and wall-bounded flows. Additional forces on the topological defects can be incorporated without altering the overall structure of the coupled system. Moreover, the specific LRT closure adopted here assumes an impermeable defect core (no penetration of the normal fluid), but this assumption is not essential: variants allowing partial penetration can be developed straightforwardly. Finally, the resulting computational framework provides a fertile arena for further numerical and algorithmic research.

(5) Self-consistent two-level closure. A central conceptual feature of the formulation is that the same LRT microhydrodynamic response generated by the line-supported coupling enters *both* sides of the problem: it closes the filtered normal-fluid equations through the residual stress and provides the filament-sampled velocity field that drives the defect dynamics. This eliminates the need for phenomenological subgrid modeling of the coupling and makes the scale-bridging fully self-consistent at the fixed cutoff scale Δ_n of turbulent fluctuations.

DATA AVAILABILITY

No data were created or analyzed in this study.

APPENDIX A: EXACT RESIDUAL-STRESS CLOSURE FROM THE LOCAL STOKES/LRT MICROFLOW

This Appendix details the explicit evaluation of the residual stress $\tau_{ij}^R = -\rho_n\, \overline{v'_{n,i} v'_{n,j}}$ appearing in the filtered normal-fluid equation, in terms of the local Stokes/LRT microflow induced by the line-supported coupling force.

1. Exact closure identity

As discussed in the main text, subfilter fluctuations are generated only by the local Stokes/LRT response $\mathbf{v}_{n,l}^S$ to the line-supported forcing. Hence,

$$\overline{v'_{n,i} v'_{n,j}}(\mathbf{x}, t) = \overline{\left(v_{n,l}^S\right)_i' \left(v_{n,l}^S\right)_j'}(\mathbf{x}, t), \tag{A1}$$

where the prime denotes the residual with respect to the filter G_{Δ_n}:

$$\overline{\mathbf{v}}_{n,l}^S(\mathbf{x}, t) = \int_\Omega \mathbf{v}_{n,l}^S(\mathbf{y}, t)\, G_{\Delta_n}(\mathbf{x} - \mathbf{y})\, d^3y, \quad \left(\mathbf{v}_{n,l}^S\right)' = \mathbf{v}_{n,l}^S - \overline{\mathbf{v}}_{n,l}^S. \tag{A2}$$

Therefore,

$$\overline{v'_{n,i} v'_{n,j}}(\mathbf{x}, t) = \int_\Omega \left(v_{n,l}^S\right)_i'(\mathbf{y}, t)\, (v_{n,l}^S)_j'(\mathbf{y}, t)\, G_{\Delta_n}(\mathbf{x} - \mathbf{y})\, d^3y. \tag{A3}$$

With the standard P3M local-global split, $\mathbf{v}_{n,l}^S$ decays rapidly beyond a splitting length chosen $O(\Delta_n)$; thus, in practice one may use $(\mathbf{v}_{n,l}^S)' \approx \mathbf{v}_{n,l}^S$ without affecting continuum-level accuracy.

2. Local Stokes/LRT field induced by line-supported forcing

Because the coupling force is supported on vortex filaments, the induced Stokes/LRT response is transversely singular around each filament and is regularized consistently at the cutoff Δ_n. We write

$$\left(v_{n,l}^S\right)_i(\mathbf{x}, t) = \int_{\mathcal{L}(t)} d\xi\; H_{ik}^{(\Delta_n)}(\mathbf{x} - \mathbf{X}(\xi, t))\, f_k^{\text{line}}(\xi, t), \tag{A4}$$

where $H^{(\Delta_n)}$ is the regularized Stokes/LRT Green tensor [[34,35], ?] compatible with the same cutoff Δ_n used in Eq. (161) and in the regularization of the line forcing in the filtered normal-fluid equation. Here $\mathbf{f}^{\rm line}(\xi, t)$ is the total force per unit arclength exerted on the normal fluid (Iordanskii plus mutual-friction contributions).

3. Cell-local evaluation and straight-segment approximation

Let $V_{\Delta_n}(\mathbf{x})$ denote the support volume of the filter G_{Δ_n} centered at $\mathbf{x}$. Since $H^{(\Delta_n)}$ is short-ranged, the local field $(v^S_{n,l})_i$ and the filtered quadratic $\overline{(v^S_{n,l})_i(v^S_{n,l})_j}$ at $\mathbf{x}$ receive contributions only from filament segments within $O(\Delta_n)$ of $\mathbf{x}$, i.e., those threading $V_{\Delta_n}(\mathbf{x})$. Accordingly, we evaluate

$$\overline{\left(v^S_{n,l}\right)_i\left(v^S_{n,l}\right)_j}(\mathbf{x}, t) = \int_{\mathbb{R}^3} \left(v^S_{n,l}\right)_i(\mathbf{x}-\mathbf{x}', t)\left(v^S_{n,l}\right)_j(\mathbf{x}-\mathbf{x}', t)\, G_{\Delta_n}(\mathbf{x}')\, d^3x'. \tag{A5}$$

Within $V_{\Delta_n}(\mathbf{x})$ each contributing filament piece is approximated by straight segments. Denote by $\{s\}$ the set of segments threading $V_{\Delta_n}(\mathbf{x})$, with center $\mathbf{X}_{s,0}(t)$, unit tangent $\mathbf{t}_s(t)$, and arclength parameter $a \in [-\ell_s/2, \ell_s/2]$:

$$\mathbf{X}_s(a, t) = \mathbf{X}_{s,0}(t) + a\,\mathbf{t}_s(t). \tag{A6}$$

Here ℓ_s denotes the arclength of segment s. Then,

$$\left(v^S_{n,l}\right)_i(\mathbf{x}, t) \;\approx\; \sum_{s\in V_{\Delta_n}(\mathbf{x})} \int_{-\ell_s/2}^{\ell_s/2} da\, H^{(\Delta_n)}_{ik}(\mathbf{x}-\mathbf{X}_s(a, t))\, f^{(s)}_k(a, t). \tag{A7}$$

4. Direct segment-based residual-stress formula

Substituting Eq. (A7) into Eq. (A5) yields an explicit segment-based representation of the residual stress $\tau^R_{ij} = -\rho_n\, \overline{v'_{n,i}v'_{n,j}}$:

$$\boxed{\tau^R_{ij}(\mathbf{x}, t) \;\approx\; -\rho_n \sum_{s\in V_{\Delta_n}(\mathbf{x})}\sum_{q\in V_{\Delta_n}(\mathbf{x})} \int_s da \int_q db\, f^{(s)}_k(a, t)\, f^{(q)}_p(b, t)\, \mathcal{K}^{kp}_{ij}(\mathbf{x}; \mathbf{X}_s(a, t), \mathbf{X}_q(b, t)),} \tag{A8}$$

where the shorthand integrals $\int_s da$ and $\int_q db$ denote $\int_{-\ell_s/2}^{\ell_s/2} da$ and $\int_{-\ell_q/2}^{\ell_q/2} db$, respectively.

The kernel $\mathcal{K}$ is the filter-weighted product of two local Green tensors evaluated over the filter neighborhood of $\mathbf{x}$:

$$\mathcal{K}^{kp}_{ij}(\mathbf{x}; \mathbf{X}_s, \mathbf{X}_q) := \int_{\mathbb{R}^3} d^3z\, G_{\Delta_n}(\mathbf{z})\, H^{(\Delta_n)}_{ik}(\mathbf{x}-\mathbf{X}_s-\mathbf{z})\, H^{(\Delta_n)}_{jp}(\mathbf{x}-\mathbf{X}_q-\mathbf{z}). \tag{A9}$$

Since $H^{(\Delta_n)}$ is short-ranged, only segment pairs separated by $O(\Delta_n)$ contribute appreciably in Eq. (A8); thus the closure remains local at the filter scale while retaining hydrodynamic interactions within the filter neighborhood.

The above equations provide an exact residual-stress closure at the continuum level defined by Δ_n: scales above Δ_n are evolved by the filtered normal-fluid solver, while the subfilter response generated by the line-supported coupling is computed from the *analytically known* (or numerically tabulated, in nonhomogeneous geometries) regularized Stokes/LRT Green tensor $H^{(\Delta_n)}$ acting on $\mathbf{f}^{\rm line}$, cf. Eqs. (A4)–(A9).

Homogeneous reduction. In translation-invariant settings (e.g., periodic domains with homogeneous filtering and local Stokes/LRT response), the kernel (A9) depends on $\mathbf{x}$, $\mathbf{X}_s$, and $\mathbf{X}_q$ only through the two relative vectors

$$\mathbf{a} := \mathbf{x} - \mathbf{X}_q, \quad \mathbf{r} := \mathbf{X}_s - \mathbf{X}_q, \tag{A10}$$

so that $\mathcal{K}^{kp}_{ij}(\mathbf{x};\mathbf{X}_s,\mathbf{X}_q)=\mathcal{K}^{kp}_{ij}(\mathbf{a},\mathbf{r})$ with

$$\mathcal{K}^{kp}_{ij}(\mathbf{a},\mathbf{r})=\int_{\mathbb{R}^3} d^3z\, G_{\Delta_n}(\mathbf{z})\, H^{(\Delta_n)}_{ik}(\mathbf{a}-\mathbf{r}-\mathbf{z})\, H^{(\Delta_n)}_{jp}(\mathbf{a}-\mathbf{z}). \tag{A11}$$

Fourier representation. Using Fourier transforms $\widehat{G}_{\Delta_n}(\mathbf{q})$ and $\widehat{H}^{(\Delta_n)}_{ik}(\mathbf{q})$, Eq. (A11) admits the exact mixed Fourier representation

$$\mathcal{K}^{kp}_{ij}(\mathbf{a},\mathbf{r})=\int \frac{d^3k}{(2\pi)^3}\, e^{i\mathbf{k}\cdot\mathbf{a}}\, \widehat{G}_{\Delta_n}(\mathbf{k}) \int \frac{d^3q}{(2\pi)^3}\, e^{-i\mathbf{q}\cdot\mathbf{r}}\, \widehat{H}^{(\Delta_n)}_{ik}(\mathbf{q})\, \widehat{H}^{(\Delta_n)}_{jp}(\mathbf{k}-\mathbf{q}). \tag{A12}$$

For incompressible screened Stokes/LRT one may take

$$\widehat{H}^{(\Delta_n)}_{ik}(\mathbf{q})=\frac{1}{\rho_n\nu}\,\frac{P_{ik}(\mathbf{q})}{q^2+\alpha^2},\quad P_{ik}(\mathbf{q})=\delta_{ik}-\frac{q_iq_k}{q^2},\quad \alpha\sim\Delta_n^{-1}, \tag{A13}$$

and for a projector (idempotent) filter one may use the sharp spectral choice $\widehat{G}_{\Delta_n}(\mathbf{q})=\mathbf{1}_{(|\mathbf{q}|<q_c)}$ with $q_c\sim\pi/\Delta_n$.

$\mathcal{K}^{kp}_{ij}$ depends only on $a=|\mathbf{a}|$, $r=|\mathbf{r}|$ and $\mu=\widehat{\mathbf{a}}\cdot\widehat{\mathbf{r}}$ and can be represented in a fixed isotropic tensor basis with scalar coefficients depending on $(a/\Delta_n, r/\Delta_n, \mu)$; these coefficients can be pretabulated. Near boundaries this reduction fails and kernel data may be tabulated from the same Stokes/LRT solver used for HI.

APPENDIX B: NONDIMENSIONALIZATION OF THE FORMAL SYSTEM

We develop here a scaling theory of the equations solved by the computational algorithm in the main text.

1. Scaling of the filtered normal-fluid dynamics

We nondimensionalize the filtered normal-fluid equation placing emphasis on the scaling of the regularized mutual-friction and Iordanskii forcings. The essential point is that two distinct small scales enter these forcings: (i) the normal-fluid filter scale Δ_n, which regularizes the distributional line forcing in the normal-fluid equations and coincides with the cutoff of the local Stokes/Linear-Response field, and (ii) the vortex arclength discretization $\delta\ell_{\rm v}\sim\ell_{\rm sd}/2$, which controls only the quadrature used to represent $\int d\xi$ along the vortex, with $\delta\ell_{\rm v}<\Delta_n$.

In addition, the forcing magnitudes are set by the relative motion between the vortex line and the normal fluid. We therefore distinguish the normal-fluid velocity scale $U_n=U$ from a characteristic vortex-line velocity scale U_L and set

$$\mathbf{v}_n=U\,\mathbf{v}_n^*,\quad \mathbf{v}_L=U_L\,\mathbf{v}_L^*,\quad \chi_L:=\frac{U_L}{U}. \tag{B1}$$

A characteristic line-normal slip magnitude is then *derived* as

$$U_{\rm slip}:=\text{typical}|\mathbf{v}_L-\mathbf{v}_n|\sim U_L+U=U(1+\chi_L) \tag{B2}$$

(up to $O(1)$ factors depending on the statistics of $\mathbf{v}_L^*$ and $\mathbf{v}_n^*$).

Transverse mutual-friction line force. In the Aristotelian transverse setting established in the main text, one has $\mathbf{t}\cdot\mathbf{v}_L=0$ and $\mathbf{t}\cdot\mathbf{v}_n(\mathbf{X})=0$, and the mutual-friction line force reduces to

$$\mathbf{f}^{\rm line}_{mf}(\xi,t)=-\nu_c(\mathbf{v}_L(\xi,t)-\mathbf{v}_n(\mathbf{X}(\xi,t),t)),\quad \nu_c:=\frac{D_\perp}{\rho_n}. \tag{B3}$$

Role of the vortex discretization scale. The line integral is evaluated on the vortex resolution scale $\delta\ell_{\mathrm{v}} \sim \ell_{\mathrm{sd}}/2$ via

$$\int d\xi\ (\cdots)\ \approx\ \sum_j \delta\ell_{\mathrm{v}}\,(\cdots)_j, \quad \delta\ell_{\mathrm{v}} < \Delta_n. \tag{B4}$$

This scale controls only quadrature convergence and is independent of the normal-fluid filter scale Δ_n.

Scaling of the filtered mutual-friction forcing. A typical magnitude of the mutual-friction force per unit length is

$$\left|\mathbf{f}_{mf}^{\mathrm{line}}\right| \sim \nu_c\, U_{\mathrm{slip}}, \quad U_{\mathrm{slip}} \sim U(1+\chi_L). \tag{B5}$$

At a point $\mathbf{x}$, the projector kernel $G_{\Delta_n}(\mathbf{x}-\mathbf{X})$ couples $\mathbf{x}$ to vortex segments lying within a neighborhood of size $O(\Delta_n)$, i.e., within a filter volume $V_\Delta(\mathbf{x}) \sim \Delta_n^3$. For a single strand threading this neighborhood, the contributing arclength is $O(\Delta_n)$, and in the filtered system $\delta\ell_{\mathrm{v}} < \Delta_n$ the number of contributing quadrature segments scales as $\Delta_n/\delta\ell_{\mathrm{v}}$ so that the quadrature factor $\delta\ell_{\mathrm{v}}$ cancels at leading order, yielding the single-strand estimate $|\mathbf{f}_{mf}^{(\Delta_n)}| \sim \nu_c U_{\mathrm{slip}}/\Delta_n^2$. In a tangle, however, $V_\Delta(\mathbf{x})$ contains a total vortex arclength $L_\Delta(\mathbf{x},t)$, and therefore an effective number of strands

$$N_\Delta(\mathbf{x},t)\ \sim\ \frac{L_\Delta(\mathbf{x},t)}{\Delta_n}, \tag{B6}$$

since each strand contributes an arclength $O(\Delta_n)$ within the filter volume. Multiplying the single-strand estimate by N_Δ gives the regularized force-per-unit-mass scale

$$\left|\mathbf{f}_{mf}^{(\Delta_n)}(\mathbf{x},t)\right| \sim \nu_c\,\frac{U_{\mathrm{slip}}}{\Delta_n^2}\,\frac{L_\Delta(\mathbf{x},t)}{\Delta_n} = \nu_c\,U_{\mathrm{slip}}\,\frac{L_\Delta(\mathbf{x},t)}{\Delta_n^3}. \tag{B7}$$

Using the definition of the local intervortex distance introduced earlier, $\delta_{iv}^{\mathrm{local}}(\mathbf{x},t) := \sqrt{V_\Delta(\mathbf{x})/L_\Delta(\mathbf{x},t)}$, one has $L_\Delta(\mathbf{x},t)/\Delta_n^3 \sim 1/(\delta_{iv}^{\mathrm{local}}(\mathbf{x},t))^2$, and thus

$$\left|\mathbf{f}_{mf}^{(\Delta_n)}(\mathbf{x},t)\right| \sim \nu_c\,\frac{U(1+\chi_L)}{\left(\delta_{iv}^{\mathrm{local}}(\mathbf{x},t)\right)^2}. \tag{B8}$$

Transverse Iordanskii line force. In the Aristotelian transverse regime the lemmas imply $\mathbf{t}\cdot\mathbf{v}_L = 0$ and $\mathbf{t}\cdot\mathbf{v}_n(\mathbf{X}) = 0$, hence the slip $\mathbf{u} := \mathbf{v}_L - \mathbf{v}_n$ satisfies $\mathbf{t}\cdot\mathbf{u} = 0$ and therefore $|\mathbf{t}\times\mathbf{u}| = |\mathbf{u}|$. The Iordanskii line force per unit length enters the normal-fluid equation as an acceleration (so that the factor ρ_n cancels) and reduces to

$$\mathbf{f}_I^{\mathrm{line}}(\xi,t) = \kappa\,\mathbf{t}(\xi,t)\times(\mathbf{v}_L(\xi,t) - \mathbf{v}_n(\mathbf{X}(\xi,t),t)). \tag{B9}$$

Scaling of the filtered Iordanskii forcing. A typical magnitude of the Iordanskii line force is

$$\left|\mathbf{f}_I^{\mathrm{line}}\right| \sim \kappa\,U_{\mathrm{slip}}, \quad U_{\mathrm{slip}} \sim U(1+\chi_L). \tag{B10}$$

Applying the same strand-counting and filtering logic as in the mutual-friction estimate, one obtains directly

$$\left|\mathbf{f}_I^{(\Delta_n)}(\mathbf{x},t)\right| \sim \kappa\,\frac{U_{\mathrm{slip}}}{\Delta_n^2}\,\frac{L_\Delta(\mathbf{x},t)}{\Delta_n} = \kappa\,U_{\mathrm{slip}}\,\frac{L_\Delta(\mathbf{x},t)}{\Delta_n^3} \sim \kappa\,\frac{U(1+\chi_L)}{\left(\delta_{iv}^{\mathrm{local}}(\mathbf{x},t)\right)^2}. \tag{B11}$$

The only difference from the mutual-friction result is the replacement $\nu_c \mapsto \kappa$, which follows because in the Aristotelian transverse regime the slip is orthogonal to the unit tangent ($\mathbf{t}\cdot\mathbf{u} = 0$ with $|\mathbf{t}| = 1$), so $|\mathbf{t}\times\mathbf{u}| = |\mathbf{u}|$ (no angle factor). Moreover, since $\kappa/\nu_c = O(1)$ in superfluid helium under the conditions considered above, the mutual-friction and Iordanskii contributions have comparable magnitudes, although the former is dissipative whereas the latter is purely reactive (redistributive).

Dimensionless filtered normal-fluid equation and effective couplings. Introducing macroscopic normal-fluid scales (L, U) via $\mathbf{x} = L\,\mathbf{x}^*$, $t = (L/U)t^*$, $\bar{\mathbf{v}}_n = U\,\bar{\mathbf{v}}_n{}^*$, and $\bar{p} = \rho_n U^2 \bar{p}^*$, together with the Reynolds number $\mathrm{Re} := UL/\nu$, the dimensionless *filtered* normal-fluid equation takes the form

$$\partial_{t^*}\bar{v}^*_{n,i} + \bar{v}^*_{n,j}\,\partial^*_j \bar{v}^*_{n,i} + \partial^*_i \bar{p}^* - \frac{1}{\mathrm{Re}}\,\partial^*_{jj}\bar{v}^*_{n,i} + \Pi_R\,\partial^*_j R^*_{ij} + \Pi_{mf}\,F^*_{mf,i}(\mathbf{x}^*, t^*) + \Pi_I\,F^*_{I,i}(\mathbf{x}^*, t^*) = 0, \tag{B12}$$

where R^*_{ij} is the dimensionless residual (subfilter) stress, defined by

$$R^*_{ij} := \frac{\overline{v'_{n,i}v'_{n,j}}}{U_R^2}, \quad R^*_{ij} = O(1), \tag{B13}$$

with U_R a characteristic subfilter velocity scale associated with the local Stokes/LRT microflow (Appendix A). The dimensionless functionals $F^*_{mf,i}$ and $F^*_{I,i}$ are $O(1)$ and encode the geometry and instantaneous slip sampled on the filament through the line laws. The corresponding effective coupling parameters scale as

$$\boxed{\Pi_{mf} \sim \frac{\nu_c}{UL}\,\frac{L^2}{\left(\delta_{iv}^{\mathrm{local}}\right)^2}\,\frac{U(1+\chi_L)}{U}, \qquad \Pi_I \sim \frac{\kappa}{UL}\,\frac{L^2}{\left(\delta_{iv}^{\mathrm{local}}\right)^2}\,\frac{U(1+\chi_L)}{U}, \qquad \Pi_R \sim \frac{L}{\Delta_n}\left(\frac{U_R}{U}\right)^2.} \tag{B14}$$

Unlike the viscous term, whose strength is fixed by the material parameters through Re, the coupling contributions depend on the evolving slip sampled on the vortex; hence, Π_{mf}, Π_I, and Π_R are *dynamic* effective couplings determined self-consistently by the coupled vortex-normal-fluid evolution. In the Aristotelian transverse regime the two line couplings differ only by the replacement $\nu_c \mapsto \kappa$. Since, as mentioned before, $\kappa/\nu_c = O(1)$ in superfluid helium, the mutual-friction and Iordanskii contributions have comparable magnitudes, although the former is dissipative whereas the latter is purely reactive (redistributive).

Remark on the role of the residual-stress term. Since $L \gg \Delta_n$ and typically $U_R \ll U$, the prefactor $\Pi_R \sim (L/\Delta_n)(U_R/U)^2$ may be small in the large-scale momentum balance. However, Π_R multiplies a stress-divergence acting at the cutoff scale, and therefore its principal impact is expected at the smallest resolved scales: even a parametrically small residual stress can contribute materially to the transfer and dissipation of kinetic energy near Δ_n. In this sense Π_R should be interpreted as a control parameter for subfilter energy exchange rather than as a measure of large-scale forcing strength.

2. Scaling of the vortex-dynamics equation

We scale the vortex-dynamics equation by estimating the magnitude of each force term and identifying the resulting dimensionless control parameters. This makes explicit the role of geometry and clarifies the origin of the overdamped (Aristotelian) limit.

Full vortex equation. The force balance per unit vortex length is

$$\rho_e\,\frac{d\mathbf{v}_L}{dt} - \rho_s\kappa\,\mathbf{t}\times(\mathbf{v}_L - \mathbf{v}_s) - \rho_n\kappa\,\mathbf{t}\times(\mathbf{v}_L - \mathbf{v}_n) - D_\parallel\,\mathbf{t}\,[\mathbf{t}\cdot(\mathbf{v}_L - \mathbf{v}_n)] - D_\perp\,\mathbf{t}\times\{\mathbf{t}\times(\mathbf{v}_L - \mathbf{v}_n)\} = \mathbf{0}. \tag{B15}$$

Geometry factors. Introduce local dimensionless factors

$$c_M := \frac{|\mathbf{t}\times(\mathbf{v}_L - \mathbf{v}_s)|}{|\mathbf{v}_L - \mathbf{v}_s|} = \sin\theta_M, \quad c_I := \frac{|\mathbf{t}\times(\mathbf{v}_L - \mathbf{v}_n)|}{|\mathbf{v}_L - \mathbf{v}_n|} = \sin\theta_I,$$
$$c_\perp := \frac{|\mathbf{t}\times\{\mathbf{t}\times(\mathbf{v}_L - \mathbf{v}_n)\}|}{|\mathbf{v}_L - \mathbf{v}_n|}, \quad c_\parallel := \frac{|\mathbf{t}\cdot(\mathbf{v}_L - \mathbf{v}_n)|}{|\mathbf{v}_L - \mathbf{v}_n|} = \cos\theta_I, \tag{B16}$$

where θ_M and θ_I are the angles between $\mathbf{t}$ and the corresponding slip velocities.

Choice of scales. We use the same macroscopic normal-fluid scales (L, U) as in the normal-fluid nondimensionalization, with $x = Lx^*$ and $t = (L/U)t^*$. We distinguish the normal-fluid velocity scale U from characteristic vortex-line and superfluid velocity scales U_L and U_S and set

$$\mathbf{v}_n = U\,\mathbf{v}_n^*, \quad \mathbf{v}_L = U_L\,\mathbf{v}_L^*, \quad \mathbf{v}_s = U_S\,\mathbf{v}_s^*, \quad \chi_L := \frac{U_L}{U}, \quad \chi_S := \frac{U_S}{U}. \tag{B17}$$

The slip magnitudes entering Eq. (B15) are then *derived* as

$$\begin{aligned} U_{Ln} &:= \text{typical}|\mathbf{v}_L - \mathbf{v}_n| \ \sim\ U_L + U = U(1+\chi_L), \\ U_{Ls} &:= \text{typical}|\mathbf{v}_L - \mathbf{v}_s| \ \sim\ U_L + U_S = U(\chi_L + \chi_S) \end{aligned} \tag{B18}$$

(up to $O(1)$ factors depending on the statistics and relative orientations of the dimensionless fields). Accordingly we scale the slips by

$$\mathbf{v}_L - \mathbf{v}_n = U_{Ln}\,\mathbf{u}_{Ln}^*, \quad \mathbf{v}_L - \mathbf{v}_s = U_{Ls}\,\mathbf{u}_{Ls}^*, \tag{B19}$$

with $\mathbf{u}_{Ln}^*, \mathbf{u}_{Ls}^* = O(1)$.

Term-by-term scaling. On the outer timescale $t = L/U$, one has

$$\left|\frac{d\mathbf{v}_L}{dt}\right| \sim \frac{U_L}{L/U} = \frac{U\,U_L}{L}. \tag{B20}$$

The magnitudes of the force terms in Eq. (B15) then scale as

$$\begin{aligned} \text{inertia:} &\quad \rho_e\,\frac{U\,U_L}{L}, \\ \text{Magnus:} &\quad \rho_s\kappa\,c_M\,U_{Ls}, \\ \text{Iordanskii:} &\quad \rho_n\kappa\,c_I\,U_{Ln}, \\ \text{longitudinal drag:} &\quad D_\parallel\,c_\parallel\,U_{Ln}, \\ \text{transverse drag:} &\quad D_\perp\,c_\perp\,U_{Ln}. \end{aligned} \tag{B21}$$

Dimensionless vortex equation. Dividing Eq. (B15) by the Magnus force scale $\rho_s\kappa U_{Ls}$ yields

$$\mathcal{I}_s\,\frac{d\mathbf{v}_L^*}{dt^*} - c_M\,\mathbf{t}\times\mathbf{u}_{Ls}^* - \chi_I\,\mathbf{t}\times\mathbf{u}_{Ln}^* - \beta_\parallel^{\text{eff}}\,\mathbf{t}\,[\mathbf{t}\cdot\mathbf{u}_{Ln}^*] - \beta_\perp^{\text{eff}}\,\mathbf{t}\times\{\mathbf{t}\times\mathbf{u}_{Ln}^*\} = \mathbf{0}, \tag{B22}$$

with the dimensionless control groups

$$\boxed{\mathcal{I}_s := \frac{\rho_e U}{\rho_s\kappa L}\,\frac{U_L}{U_{Ls}}, \quad \chi_I := \chi_n\,c_I\,\frac{U_{Ln}}{U_{Ls}}, \quad \beta_\parallel^{\text{eff}} := \beta_\parallel\,c_\parallel\,\frac{U_{Ln}}{U_{Ls}}, \quad \beta_\perp^{\text{eff}} := \beta_\perp\,c_\perp\,\frac{U_{Ln}}{U_{Ls}}.} \tag{B23}$$

Here $\chi_n := \rho_n/\rho_s$, $\beta_\parallel := D_\parallel/(\rho_s\kappa)$, and $\beta_\perp := D_\perp/(\rho_s\kappa)$, while U_{Ln} and U_{Ls} are the derived slip scales in Eq. (B18), and $c_M, c_I, c_\parallel, c_\perp$ are the local geometry factors defined above.

Application of the lemmas. In the Aristotelian regime considered here, the lemmas established earlier imply that the relevant velocities sampled on the filament are transverse, so that $\mathbf{t}\cdot\mathbf{u}_n = 0$ (and similarly for the Magnus slip), hence

$$c_\parallel = 0, \quad c_M = c_I = c_\perp = 1. \tag{B24}$$

All explicit $\sin\theta$ factors therefore drop out of the *magnitudes* of the coupling forces: The local tangle geometry affects only force directions, not their strength.

Overdamped (Aristotelian) limit. For helium II, $\rho_e \sim \rho_s a_0^2$ is extremely small, so that $\mathcal{I}_s \ll 1$ on all macroscopic scales. The inertial term therefore relaxes on a microscopic time and can be neglected for continuum dynamics. The vortex motion is then determined instantaneously by the algebraic balance between the Magnus term and the normal-fluid coupling terms (Iordanskii and transverse mutual friction), with the derived slip scales $U_{Ln} \sim U_L + U$ and $U_{Ls} \sim U_L + U_S$ set self-consistently by the coupled evolution.

[1] M. Guidry and Y. Sun, *Symmetry, Broken Symmetry, and Topology in Modern Physics* (Cambridge University Press, Cambridge, UK, 2022).
[2] T. Lancaster and S. J. Blundell, *Quantum Field Theory for the Gifted Amateur* (Oxford University Press, Oxford, UK, 2014).
[3] A. J. Legget, *Quantum Liquids: Bose Condensation and Cooper Pairing in Condensed-Matter Systems* (Oxford University Press, Oxford, UK, 2006).
[4] E. Zaremba, A. Griffin, and T. Nikuni, *Bose-Condensed Gases at Finite Temperatures* (Cambridge University Press, Cambridge, UK, 2009).
[5] G. E. Volovik, *The Universe in a Helium Droplet* (Oxford University Press, Oxford, UK, 2003).
[6] M. A. Schlosshauer, *Decoherence: And the Quantum-to-Classical Transition* (Springer, Berlin, 2007).
[7] R. L. Liboff, *Kinetic Theory: Classical, Quantum, and Relativistic Descriptions* (Springer, Berlin, 2003).
[8] K. Morawetz, *Interacting Systems Far from Equilibrium: Quantum Kinetic Theory* (Oxford University Press, Oxford, UK, 2017).
[9] P. Attard, *Non-Equilibrium Thermodynamics and Statistical Mechanics: Foundations and Applications* (Oxford University Press, Oxford, UK, 2012).
[10] R. J. Donnelly, *Quantized Vortices in Helium II* (Cambridge University Press, Cambridge, UK, 2008).
[11] S. K. Nemirovskii, Quantum turbulence: Theoretical and numerical problems, Phys. Rep. **524**, 85 (2013).
[12] Edited by C. F. Barenghi and R. J. Donnelly, *Quantized Vortex Dynamics and Superfluid Turbulence* (Springer, Berlin, 2010).
[13] W. F. Vinen, Mutual friction in a heat current in liquid helium II. II. Experiments on transient effects, Proc. R. Soc. London, Ser. A **240**, 128 (1957).
[14] W. F. Vinen, Mutual friction in a heat current in liquid helium II. III. Theory of the mutual friction, Proc. R. Soc. London, Ser. A **242**, 493 (1957).
[15] G. E. Volovik, Three nondissipative forces on a moving vortex line in superfluids and superconductors, Pis'ma Zh. Eksp. Teor. Fiz. **62**, 58 (1995).
[16] K. W. Schwarz, Three-dimensional vortex dynamics in superfluid ^{4}He: Line-line and line-boundary interactions, Phys. Rev. B **31**, 5782 (1985).
[17] E. B. Sonin, *Dynamics of Quantised Vortices in Superfluids* (Cambridge University Press, Cambridge, UK, 2016).
[18] P. M. Walmsley and A. I. Golov, Quasiclassical and ultraquantum decay of superfluid turbulence, Phys. Rev. Lett. **100**, 245301 (2008).
[19] D. Kivotides, Mutual-friction induced instability of normal-fluid vortex tubes in superfluid helium-4, Phys. Lett. A **382**, 1481 (2018).
[20] S. K. Nemirovskii, On the closure problem of the coarse-grained hydrodynamics of turbulent superfluids, J. Low Temp. Phys. **201**, 254 (2020).
[21] D. Kivotides, Superfluid hydrodynamics with discrete topological defects, Phys. Rev. Fluids **3**, 104701 (2018).
[22] L. Galantucci, A. W. Baggaley, C. F. Barenghi, and G. Krstulovic, A new self-consistent approach of quantum turbulence in superfluid helium, Eur. Phys. J. Plus **135**, 547 (2020).
[23] C. Pozrikidis, *Boundary Integral and Singularity Methods for Linearized Viscous Flow* (Cambridge University Press, Cambridge, UK, 1992).
[24] E. Guazzelli and J. F. Morris, *A Physical Introduction to Suspension Dynamics* (Cambridge University Press, Cambridge, UK, 2011).
[25] E. G. Sinaiski and L. I. Zaichik, *Statistical Microhydrodynamics* (Wiley-VCH, Weinheim, 2008).
[26] P. Oswald, *Rheophysics: The Deformation and Flow of Matter* (Cambridge University Press, Cambridge, UK, 2009).
[27] D. C. Samuels and D. Kivotides, A damping length scale for superfluid turbulence, Phys. Rev. Lett. **83**, 5306 (1999).
[28] L. Thompson and P. C. E. Stamp, Quantum dynamics of a Bose superfluid vortex, Phys. Rev. Lett. **108**, 184501 (2012).
[29] G. Baym and E. Chandler, The hydrodynamics of rotating superfluids. I. Zero-temperature, nondissipative theory, J. Low Temp. Phys. **50**, 57 (1983).

[30] T. I Dauxois and M. Peyrard, *Physics of Solitons* (Cambridge University Press, Cambridge, UK, 2006).

[31] M. Doi, *Soft Matter Physics* (Oxford University Press, Oxford, UK, 2013).

[32] N. A. Lemos, *Analytical Mechanics* (Cambridge University Press, Cambridge, UK, 2018).

[33] W. E. Gurtin, E. Fried, and L. Anand, *The Mechanics and Thermodynamics of Continua* (Cambridge University Press, Cambridge, UK, 2010).

[34] L. G. Leal, *Advanced Transport Phenomena: Fluid Mechanics and Convective Transport Processes* (Cambridge University Press, Cambridge, UK, 2007).

[35] M. D. Graham, *Microhydrodynamics, Brownian Motion, and Complex Fluids* (Cambridge University Press, Cambridge, UK, 2018).

[36] R. W Hockney and J. W Eastwood, Computer simulation using particles (CRC Press, Boca Raton, FL, 1988).

[37] J. Happel and H. Brenner, *Low Reynolds Number Hydrodynamics* (Kluwer Academic Publishers, Dordrecht, 1977).

[38] A. T. A. M. de Waele and R. G. K. M. Aarts, Route to vortex reconnection, Phys. Rev. Lett. **72**, 482 (1994).

[39] K. W. Schwarz, Three-dimensional vortex dynamics in superfluid ^{4}He: Homogeneous superfluid turbulence, Phys. Rev. B **38**, 2398 (1988).

[40] D. C. Samuels, Velocity matching and Poiseuille pipe flow of superfluid helium, Phys. Rev. B **46**, 11714 (1992).

[41] M. Tsubota, T. Araki, and S. K. Nemirovskii, Dynamics of vortex tangle without mutual friction in superfluid ^{4}He, Phys. Rev. B **62**, 11751 (2000).

[42] H. Adachi, S. Fujiyama, and M. Tsubota, Steady-state counterflow quantum turbulence: Simulation of vortex filaments using the full Biot-Savart law, Phys. Rev. B **81**, 104511 (2010).

[43] L. Kondaurova and S. K. Nemirovskii, Full Biot-Savart numerical simulation of vortices in He II, J. Low Temp. Phys. **138**, 555 (2005).

[44] P. Davidson, *Turbulence* (Oxford University Press, Oxford, UK, 2004).

[45] D. Kivotides, A method for the computation of turbulent polymeric liquids including hydrodynamic interactions and chain entanglements, Phys. Lett. A **381**, 629 (2017).